~~PROSPECTIVE~~ NASA CR 137762

Final Report

MEASUREMENTS OF TRACE CONSTITUENTS FROM ATMOSPHERIC INFRARED EMISSION AND ABSORPTION SPECTRA - A FEASIBILITY STUDY

A. Goldman, W. J. Williams and D. G. Murcray

September 1974

Prepared under Contract No. NAS2-8200

by

Department of Physics and Astronomy
University of Denver
Denver, Colorado 80210

for

AMES RESEARCH CENTER
NATIONAL AERONAUTICS AND SPACE ADMINISTRATION

PROSPECTIVE NASA CR

Final Report

MEASUREMENTS OF TRACE CONSTITUENTS FROM ATMOSPHERIC INFRARED EMISSION AND ABSORPTION SPECTRA - A FEASIBILITY STUDY

A. Goldman, W. J. Williams and D. G. Murcray

September 1974

Prepared under Contract No. NAS2-8200

by

Department of Physics and Astronomy
University of Denver
Denver, Colorado 80210

for

AMES RESEARCH CENTER
NATIONAL AERONAUTICS AND SPACE ADMINISTRATION

Measurements of Trace Constituents from Atmospheric Infrared Emission and Absorption Spectra - A Feasibility Study

by

A. Goldman, W. J. Williams and D. G. Murcray
Department of Physics and Astronomy
University of Denver
Denver, Colorado 80210

Abstract

The feasibility of detecting eight trace constituents (CH_4, HCl, HF, HNO_3, NH_3, NO, NO_2 and SO_2) against the rest of the atmospheric background at various altitudes from infrared emission and absorption atmospheric spectra has been studied. Line-by-line calculations and observational data have been used to establish features that can be observed in the atmospheric spectrum due to each trace constituent. Model calculations have been made for experimental conditions which approximately represent "state of the art" emission and absorption spectrometers.

TABLE OF CONTENTS

I. Introduction

Infrared methods are very powerful techniques for trace gas measurement due to the unique patterns in the fine structure of the spectral lines of both the background atmosphere and trace constituents. The enormous amount of work of many individuals during the last decade has resulted in extensive tabulations of spectral line parameters of a number of gases. During that time, efficient line-by-line computer programs have been developed which, with today's large computers, allow the generation of synthetic atmospheric spectra for arbitrary atmospheric profiles of minor constituents with arbitrary optical paths and spectral resolutions. While these techniques have been extensively used for the analysis of observed atmospheric emission and absorption infrared spectra, their use in feasibility studies for infrared measurements of atmospheric trace constituents[1-18] was quite limited.

When small amounts of gas are to be measured, accurate knowledge is required of the fine details of both the experiment and the theory. In particular, the effects of interference between various molecular features that might be present in the spectrum require special attention. The line-by-line techniques are very powerful in such cases, as is demonstrated in a recent study of the solar spectrum during a search for stratospheric NO.[19] It was shown that a detailed line-by-line analysis of interferences is a basic requirement for a meaningful determination of minor constituents from weak spectral features.

A similar problem occurs with many other gases in various spectral regions. Therefore, in the present work we have applied the line-by-line techniques to the problem of finding detectable limits for a number of trace constituents against the rest of the atmospheric background. In particular, we have studied the effects of interference on the detectability of small amounts of CH_4, HCl, HF, HNO_3, NH_3, NO, NO_2 and SO_2 under

conditions corresponding to selected practical atmospheric experiments with absorption and emission spectrometers.

II. Calculation Procedure

In the present calculations a one-layer model of the atmosphere was used with appropriate effective temperature, pressure and mixing ratio to determine the optical path. The effective mixing ratios for the minor constituents of the background atmosphere were derived from the AFCRL mid-latitude summer profile.[20]

The spectra were calculated on a line-by-line basis using the most recently available line parameters for the various molecular species. The line parameters for the background atmosphere are those generated by various researchers (notably by W.S. Benedict) and compiled on magnetic tape by AFCRL.[21] These cover most of the relevant bands of H_2O, CO_2, O_3, N_2O, CH_4, CO and O_2. Additional line parameters that were generated at the University of Denver and elsewhere for the strongest bands of HCl,[22] HF,[23] NH_3,[24] NO,[25] NO_2,[26] and SO_2[27, 28] were used for the calculations of the spectra of the background atmosphere with the additional constituents. A Voigt line shape was used for all spectral lines.

It should be noted that the calculated background spectra presented here do not include the HNO_3 vibration-rotation bands, the H_2O vapor continuum and the pressure-induced bands of O_2 and N_2. Deviations from the Voigt line shape are also neglected here. In addition, solar molecular and atomic lines, which can cause significant interference with atmospheric lines in actual atmospheric spectra taken with the sun as a source, have not been included. The corresponding NO and HF spectra presented here should have been thus superimposed on the solar CO $\Delta v=1$ and $\Delta v=2$ transitions respectively.

The effects of interference between solar CO lines and atmospheric NO lines has been studied earlier.[19] In addition, numerous atomic solar lines occur in the vicinity of the HF and HCl lines presented here. The effects of these lines on the presently used HF and HCl lines are discussed here only briefly because the subject requires a separate detailed study. Furthermore, it should be noted that for a constituent which is layered sharply at a certain altitude, the constant mixing ratio assumed for the trace constituents added to the background atmosphere makes the present charts less accurate.

The calculations were performed so as to correspond to three different experimental techniques; long path absorption cell with laser spectroscopy, atmospheric absorption spectra using the sun as a source and atmospheric emission spectra. The calculations were performed for "infinite" resolution and the resolution was then degraded to correspond to resolutions of 0.08 cm^{-1} and 1.0 cm^{-1}, which are close to current "state of the art" of each experimental technique. Examples of each technique are found in the literature.[1-19, 29-39] The absorption data were combined with the appropriate blackbody function to get the atmospheric emission data. Four altitudes were chosen as the base of each atmospheric layer: 5.5 km, 15 km, 25 km and 35 km. These were chosen to represent the upper troposphere, near of just above the tropopause, the ozone layer and the middle stratosphere where photochemical effects dominate. The main advantage of solar spectroscopy and atmospheric emission spectra lies in the large optical path which is achieved at large zenith angles. These calculations were therefore performed for zenith angles at 80° and 85°. For laser spectroscopy with a long path cell, a cell of 100 meters was chosen for all cases except for CH_4 where shorter cells were chosen.

III. Results

The theoretical calculations are presented in graphical form showing either radiance or emissivity as a function of wavelength and wavenumber. The calculations are presented according to molecule, altitude and the three experimental techniques discussed above. In most cases the data are plotted on both logarithmic and linear scales to demonstrate graphically how the limit of detectability depends on the dynamic range which can be achieved with the observational technique employed. In each case the atmospheric background spectrum is plotted on the same figure with the spectrum of background plus the trace constituent. The stronger features of the particular trace constituent are denoted by vertical or horizontal arrows. The vertical scales of these plots are offset for clarification. In addition, the experimental conditions are denoted on each figure and include the spectral resolution, the altitude and the optical path.

When either logarithmic or linear plots are shown on a chart, the scales on the left and on the right sides apply to the atmosphere with and without the trace constituent respectively. When both logarithmic and linear plots are shown on the same chart, the log and the linear scales are on the left and the right sides respectively. In these cases, the upper and the lower scales apply to the atmosphere with and without the trace constituent respectively.

The spectral calculations for each trace constituent and the associated specific discussions pertaining to each species are found below in separate sections. Detectable amounts of the individual molecules are discussed on the basis of the atmospheric emission and absorption spectra calculated in Figures 1 through 34. In preparing these figures the criterion for a measurable absorptivity was taken as ~1%. The measurable radiance level depends on the wavelength region and is discussed for each molecule separately.

III. A. CH_4

The natural abundance of CH_4 in the lower stratosphere is of the order of 0.1 to 1.0 ppmv. Such a mixing ratio is larger than the mixing ratios of all the other molecules considered in the present report, as the others are trace gases to be measured against the rest of the atmospheric gases. As a result, a relatively short path length and medium resolution can be used for atmospheric CH_4 measurements, either from the solar spectrum or from the atmospheric emission spectrum. A large number of such spectra have been observed from various altitudes, with the most intense CH_4 features occurring in the 3.3μm and the 7.6μm regions. Therefore in the present report these two regions are considered only for laser spectroscopy with an absorption cell. The calculated CH_4 absorptions presented here are weak and allow linear scaling of gas amount and absorption up to ~10% absorption.

"Infinite" resolution atmospheric absorption calculations for a 5 meter path for both the 3.3μm and 7.6μm Q-branch regions, at 5.5 km altitude, are shown in Figures 1 and 2 and Figure 3 respectively. Assuming ~1% measurable absorptivity allows the measurement of ~0.5 ppmv CH_4 under these conditions. It is seen that both CH_4 regions are subject to significant interference from atmospheric lines, but the interference is less in the 3.3μm region.

Similar "infinite" resolution calculations at 25 km altitude for a 40 meter path near 3.3μm and a 20 meter path near 7.6μm are shown in Figures 4 and 5 and Figure 6 respectively. Scaling these figures to ~1% measurable absorptivity allows the measurement of ~0.5 ppmv CH_4 with an ~20 meter cell from either region. It is noted that while the atmospheric interference is now practically negligible for the 3.3μm region (where the numerous atmospheric lines are lower in absorption intensity by orders of magnitude in comparison with the CH_4 lines),

the 7.6μm CH_4 lines are superimposed on many atmospheric lines with absorption intensity comparable to that of the CH_4 lines.

The line parameters for CH_4 and the atmosphere are relatively accurate in both spectral regions. It should be noted, however, that the Q-branch CH_4 lines are subject to uncertainties, but their accumulated intensity permits a lower detectable limit than that for P- and R-branch lines.

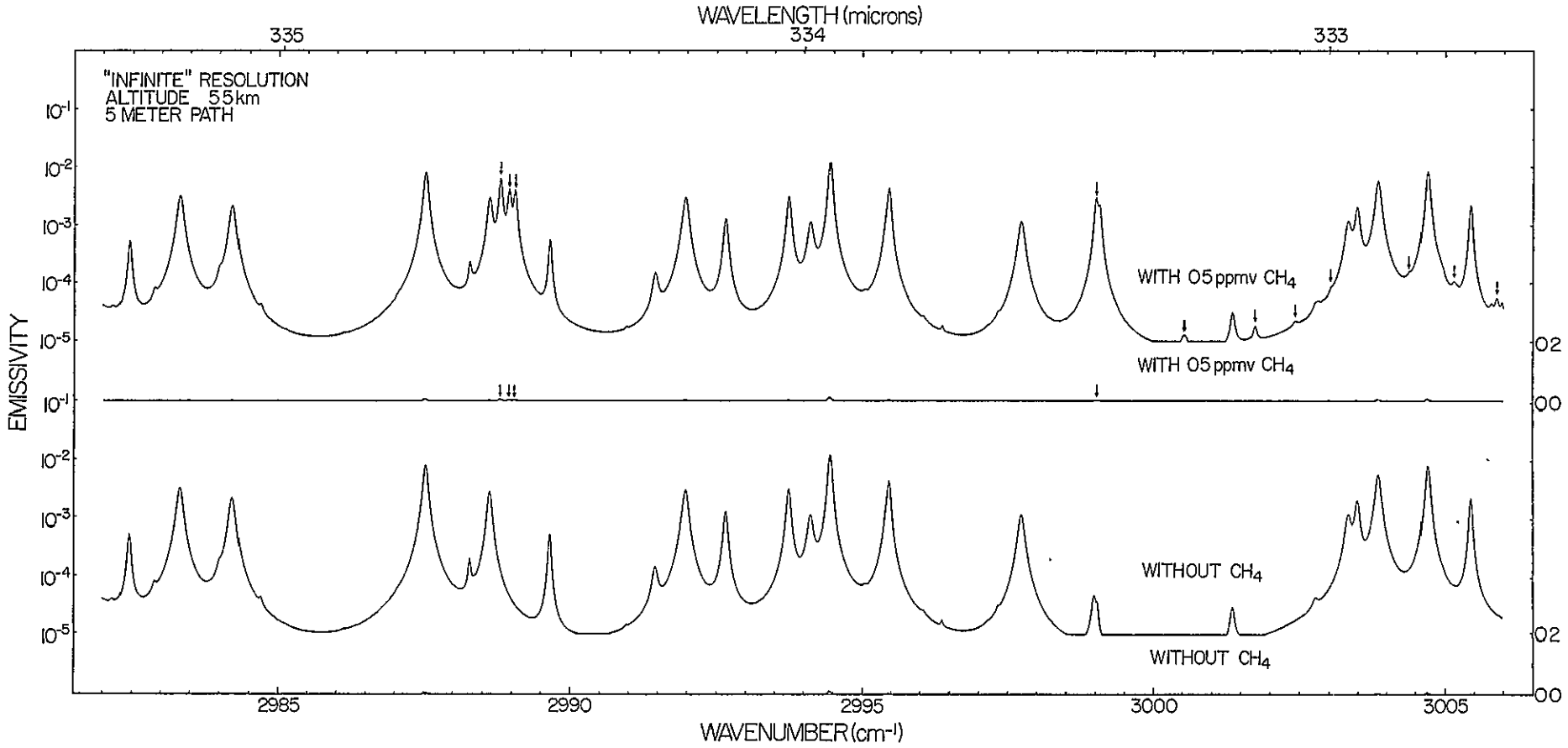
WAVELENGTH (microns)
335
334
333
"INFINITE" RESOLUTION
ALTITUDE 5.5km
5 METER PATH
EMISSIVITY
WITH 05 ppmv CH4
WITH 05 ppmv CH4
WITHOUT CH4
WITHOUT CH4
02
00
02
00
2985
2990
2995
3000
3005
WAVENUMBER (cm-1)

Figure 1.

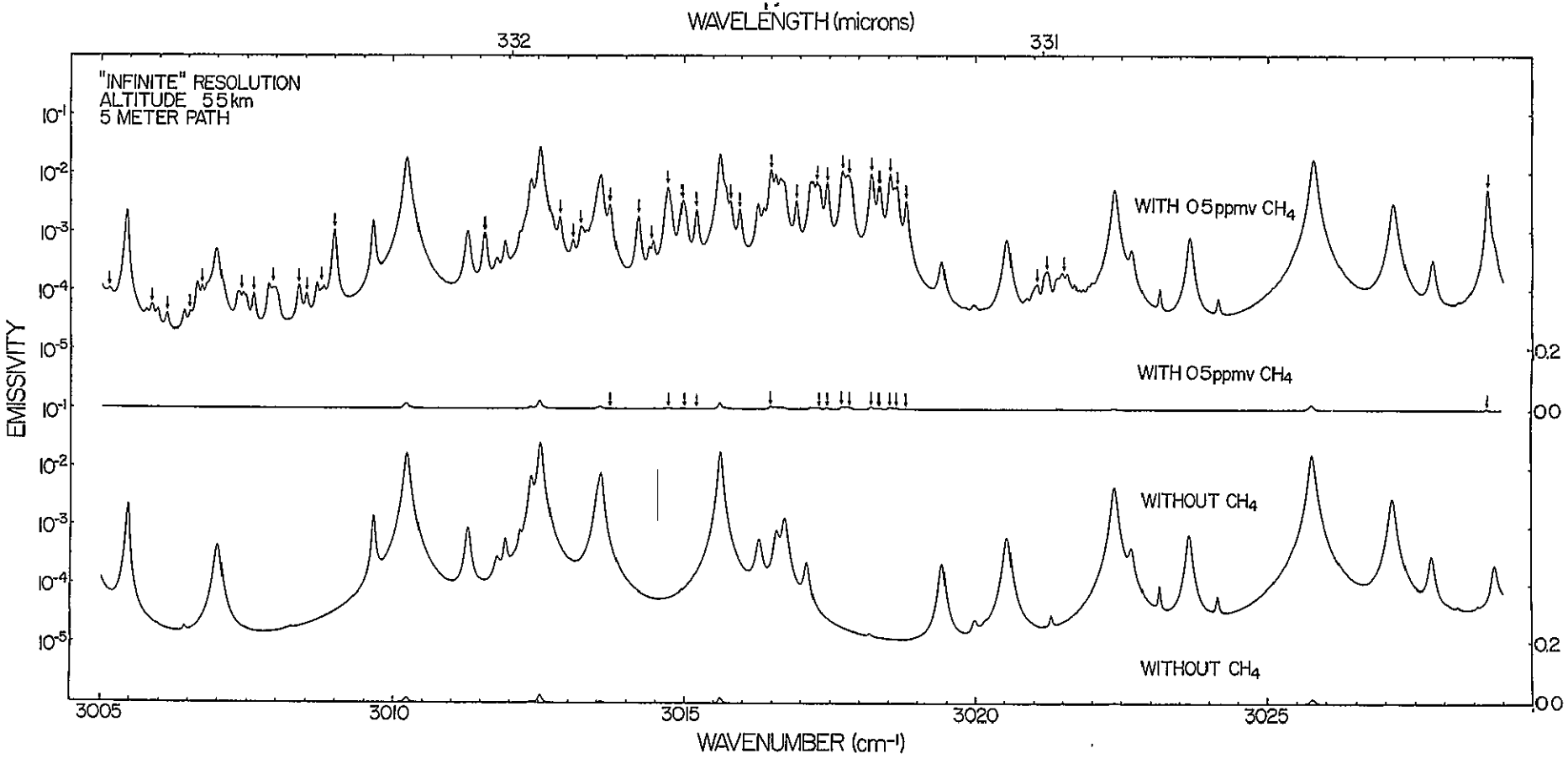
WAVELENGTH (microns)
332
331
"INFINITE" RESOLUTION
ALTITUDE 55km
5 METER PATH
WITH 05ppmv CH4
WITH 05ppmv CH4
WITHOUT CH4
WITHOUT CH4
EMISSIVITY
10-1
10-2
10-3
10-4
10-5
0.2
0.0
0.2
0.0
3005
3010
3015
3020
3025
WAVENUMBER (cm-1)

Figure 2.

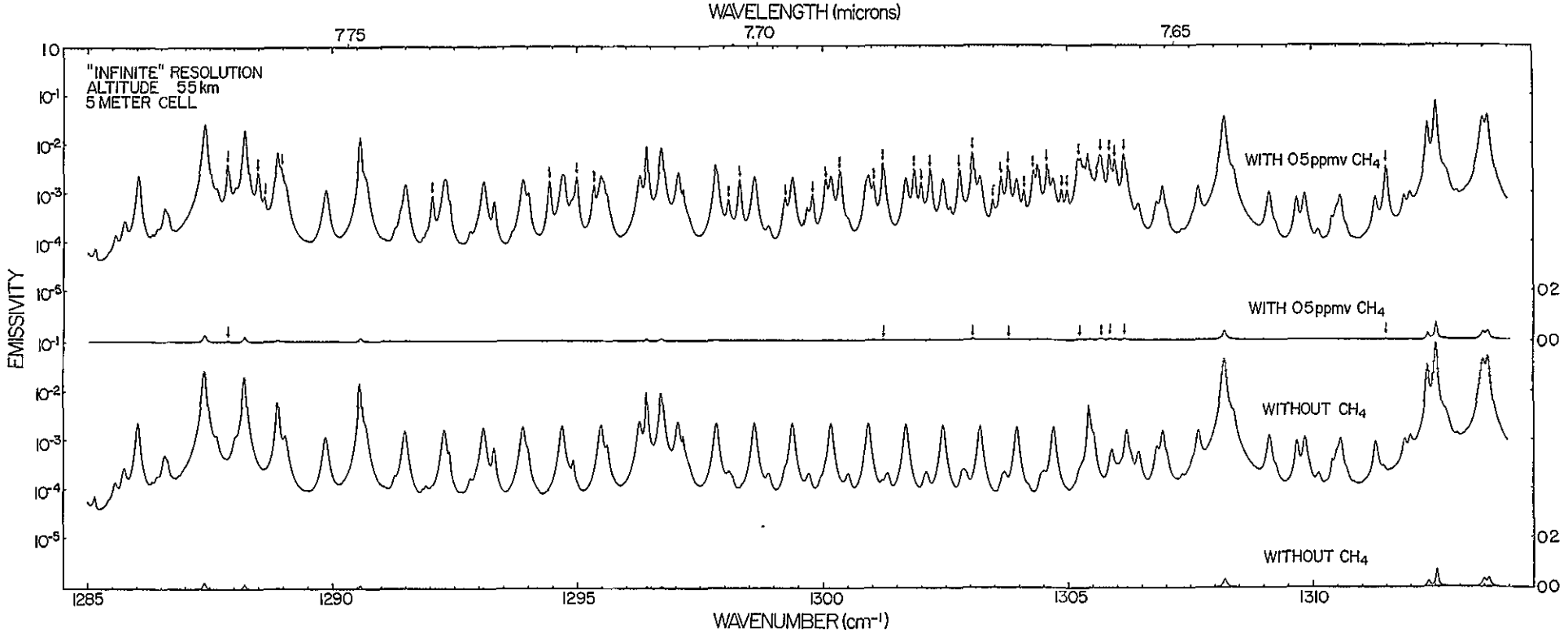
WAVELENGTH (microns)
7.75
7.70
7.65
"INFINITE" RESOLUTION
ALTITUDE 55 km
5 METER CELL
WITH 05ppmv CH4
WITH 05ppmv CH4
WITHOUT CH4
WITHOUT CH4
EMISSIVITY
1285
1290
1295
1300
1305
1310
WAVENUMBER (cm-1)

Figure 3.

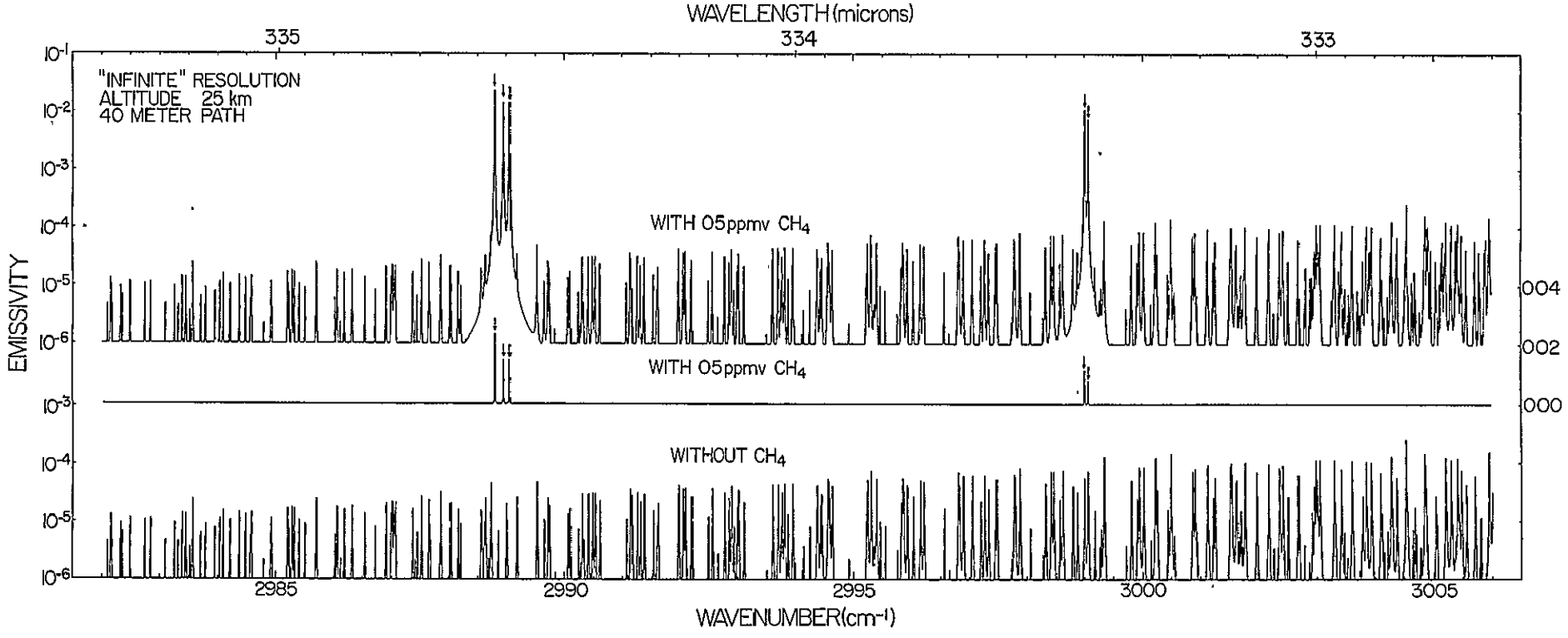
WAVELENGTH (microns)
335
334
333
"INFINITE" RESOLUTION
ALTITUDE 25 km
40 METER PATH
WITH 05ppmv CH4
WITH 05ppmv CH4
WITHOUT CH4
EMISSIVITY
10-1
10-2
10-3
10-4
10-5
10-6
10-3
10-4
10-5
10-6
004
002
000
2985
2990
2995
3000
3005
WAVENUMBER(cm-1)

Figure 4.

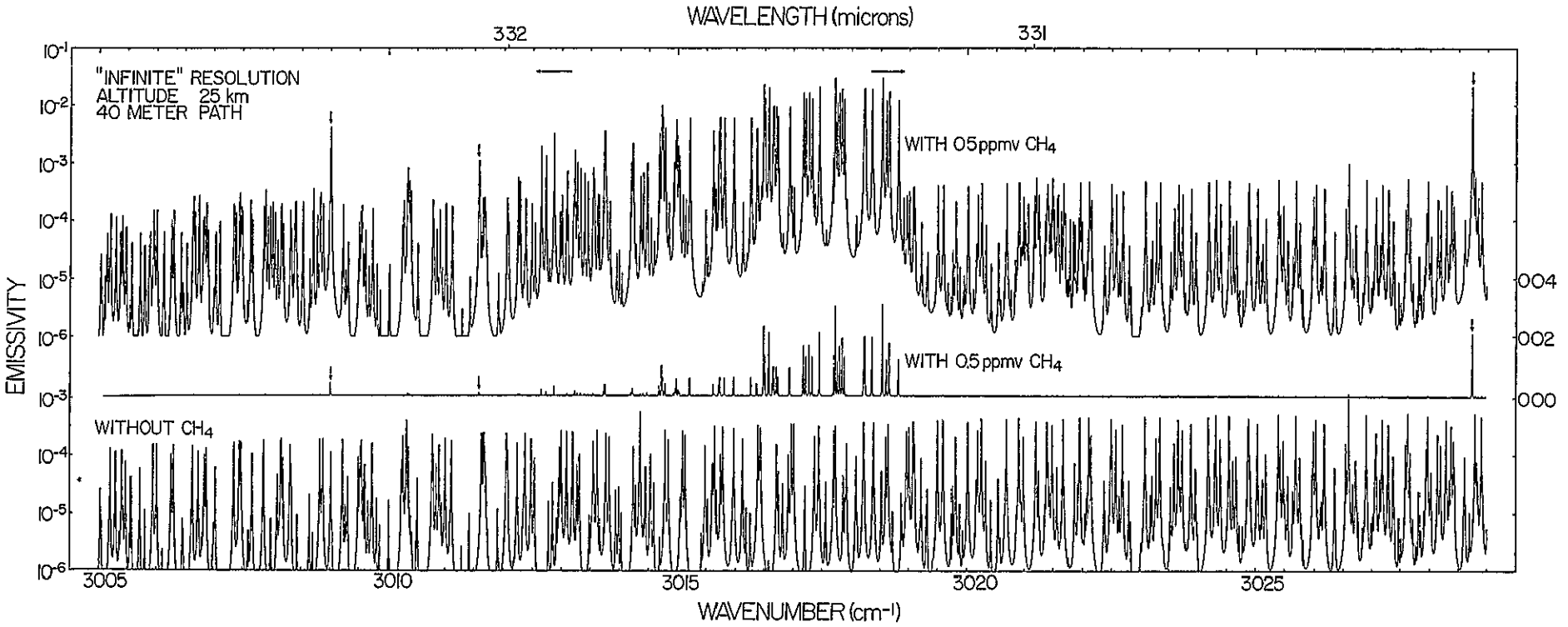
WAVELENGTH (microns)
332
331
"INFINITE" RESOLUTION
ALTITUDE 25 km
40 METER PATH
WITH 0.5 ppmv CH4
WITH 0.5 ppmv CH4
WITHOUT CH4
EMISSIVITY
10-1
10-2
10-3
10-4
10-5
10-6
004
002
000
3005
3010
3015
3020
3025
WAVENUMBER (cm-1)

Figure 5.

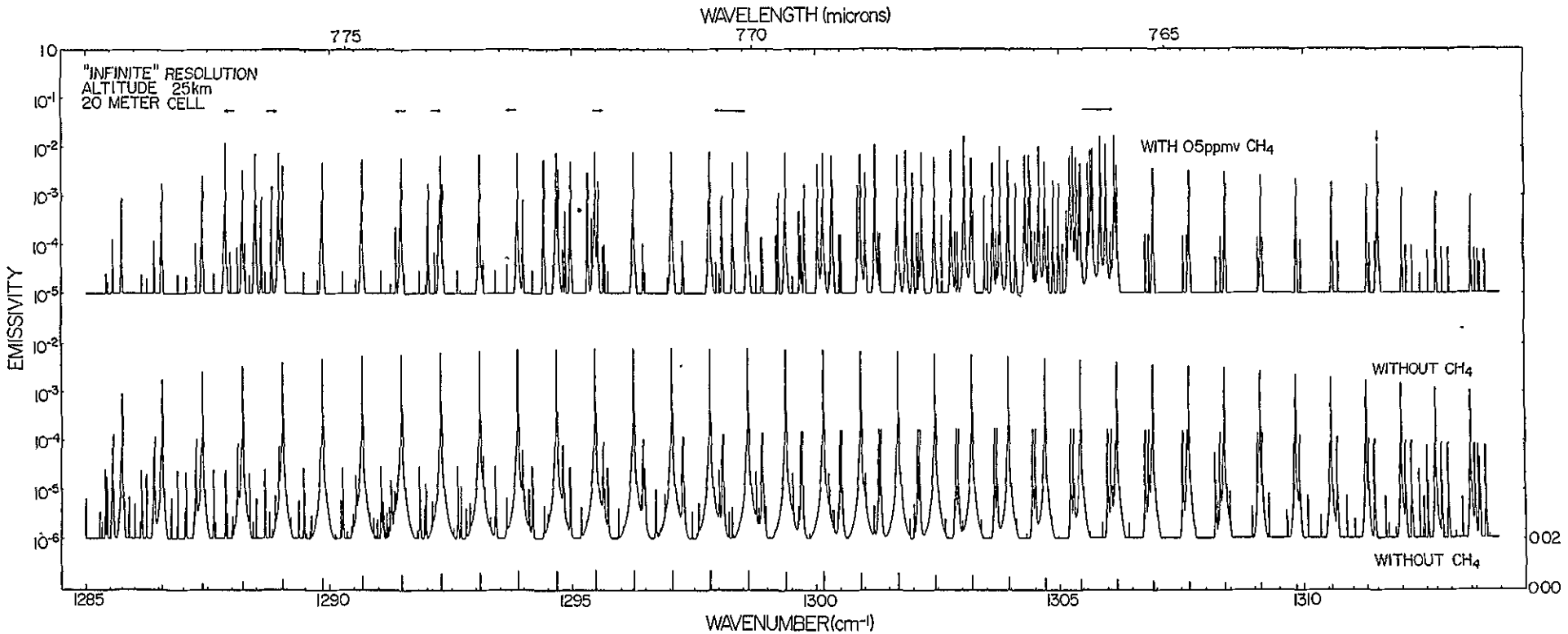
WAVELENGTH (microns)
775
770
765
"INFINITE" RESOLUTION
ALTITUDE 25km
20 METER CELL
WITH 05ppmv CH4
WITHOUT CH4
WITHOUT CH4
EMISSIVITY
10
10-1
10-2
10-3
10-4
10-5
10-2
10-3
10-4
10-5
10-6
002
000
1285
1290
1295
1300
1305
1310
WAVENUMBER(cm-1)

Figure 6.

III. B. HCl

The (0-1) vibration-rotation band of HCl offers several possibilities for HCl detection.

"Infinite" resolution atmospheric absorption calculations for a 100 meter path at 5.5 km and 15 km altitudes are shown in Figures 7 through 9. Assuming an ~1% measurable absorptivity allows the measurement of ~10 ppbv and ~20 ppbv HCl at 5.5 and 15 km by scaling these figures to ~1% emissivity. It is seen that in the spectral region under consideration there is practically no interference from atmospheric lines for a 100 meter path.

Atmospheric spectral radiance calculated with and without HCl for 15 km altitude, 80° zenith angle and 1 cm^{-1} resolution is shown in Figures 10 and 11. It is seen that 1 ppbv of HCl gives rise to a number of HCl features superimposed on the atmospheric spectrum. The radiance levels shown for the HCl features at $\sim 2 \times 10^{-9}$ w cm^{-2} sr^{-1} μm^{-1} are at the lower limit of "state of the art" spectral radiometers at 3.5μm.

By dividing the radiance signal by the blackbody signal, the above radiance figures yield an absorptivity of ~1%. Therefore, a solar spectrum taken under these conditions (15 km altitude, 80° zenith angle and 1 cm^{-1} resolution) will allow the measurement of ~1 ppbv HCl. Such spectra are easily obtained with current solar spectrometers.

Absorption spectra as would be expected in solar spectrum measurements from 25 km at 85° zenith angle and 0.08 cm^{-1} resolution, are calculated in Figures 12 through 14 for two spectral regions. From Figures 12 and 13 it is seen that the HCl isotopic lines near 2945 cm^{-1} are well separated from the atmospheric lines. Absorptivity of ~1% allows the measurement of ~0.1 ppbv HCl. A comparison of Figures 12 and 13 and Figure 14 shows that the 2945 cm^{-1} region is more useful than the 2820 cm^{-1} region for HCl measurements in the atmosphere.

While the intensities of the HCl lines in the two spectral regions are quite similar, the interference from the atmospheric lines is significantly smaller in the 2945 cm^{-1} region.

The line parameters for HCl and the atmosphere are relatively accurate in the 3.4μm region. However, closer attention should be given to the solar background lines for solar spectra measurements in the HCl region where several atomic lines have been observed.[39]

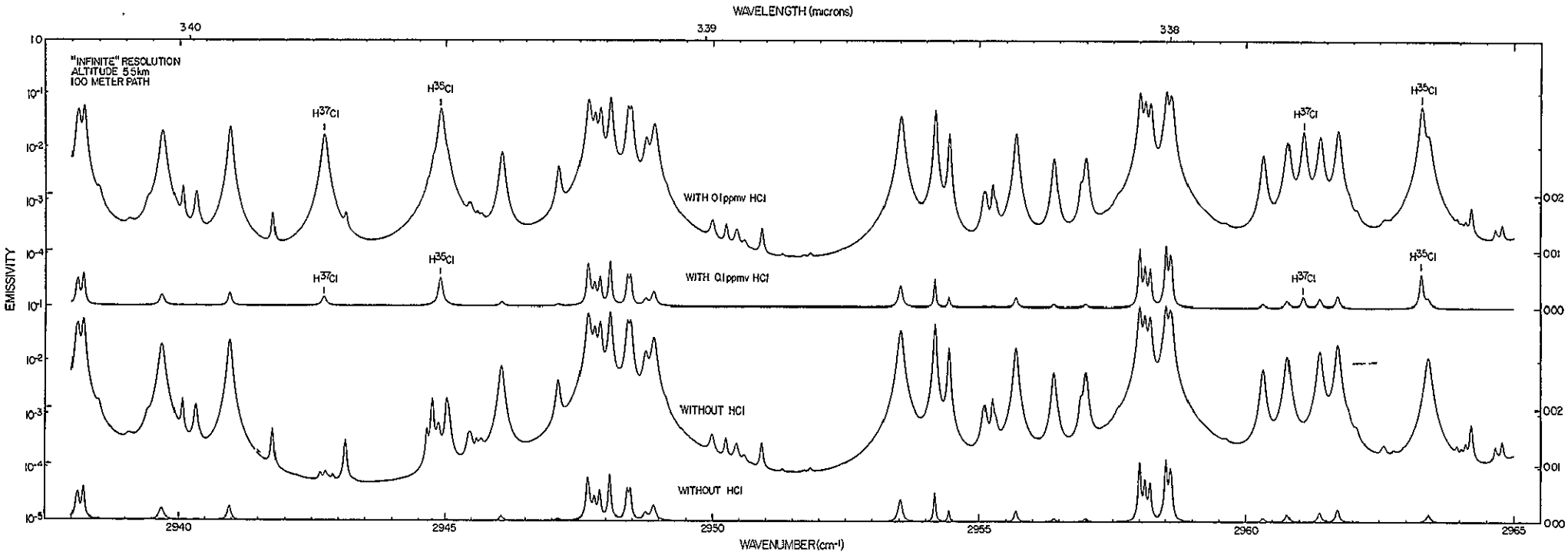
WAVELENGTH (microns)
3.40
3.39
3.38
"INFINITE" RESOLUTION
ALTITUDE 55km
100 METER PATH
H37Cl
H35Cl
WITH 0.1ppmv HCl
WITH 0.1ppmv HCl
WITHOUT HCl
WITHOUT HCl
EMISSIVITY
2940
2945
2950
2955
2960
2965
WAVENUMBER(cm-1)

Figure 7.

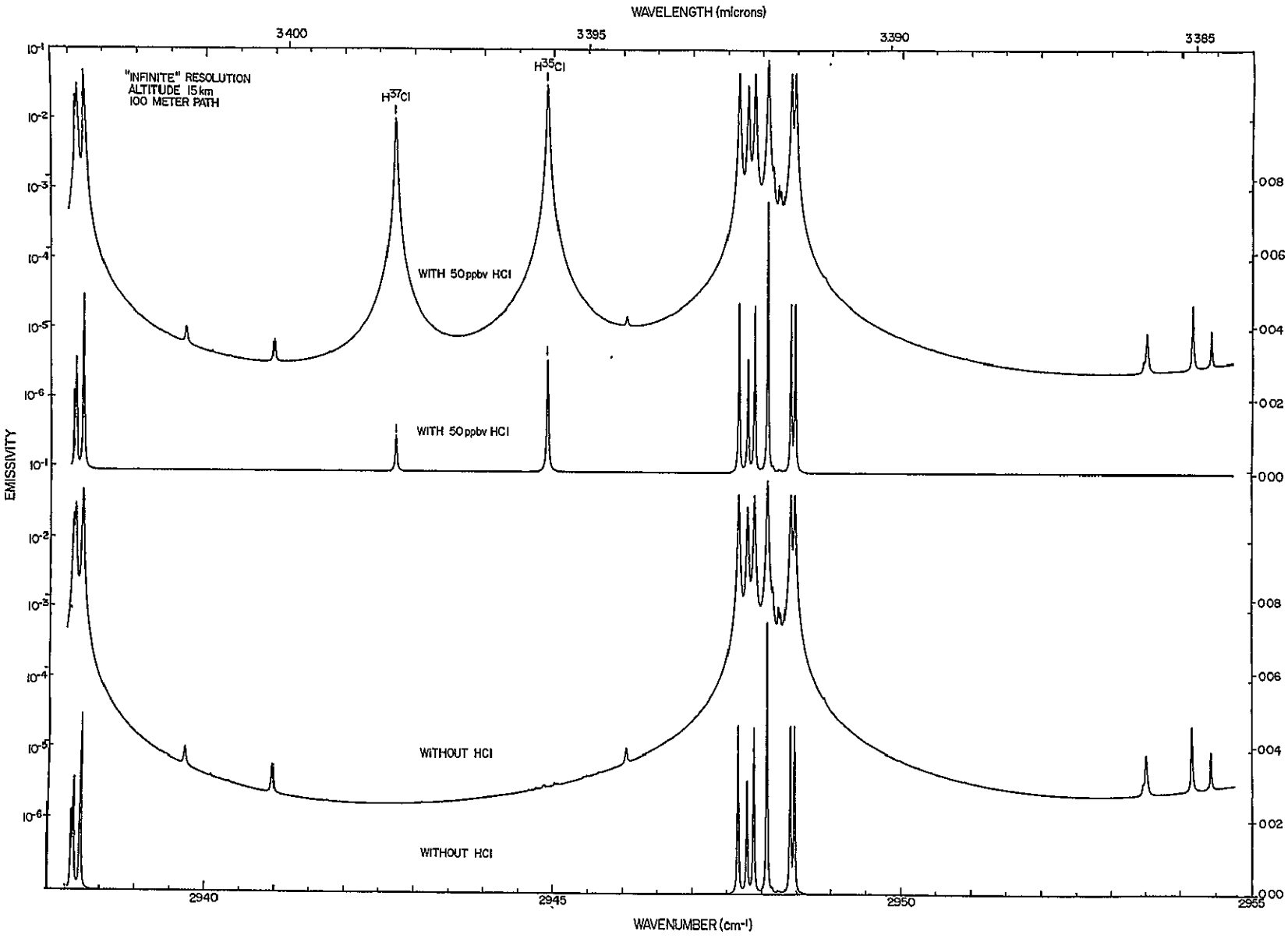
WAVELENGTH (microns)
3400
3395
3390
3385
"INFINITE" RESOLUTION
ALTITUDE 15 km
100 METER PATH
H37Cl
H35Cl
WITH 50ppbv HCl
WITH 50ppbv HCl
WITHOUT HCl
WITHOUT HCl
EMISSIVITY
10-1
10-2
10-3
10-4
10-5
10-6
.008
.006
.004
.002
.000
2940
2945
2950
2955
WAVENUMBER (cm-1)

Figure 8.

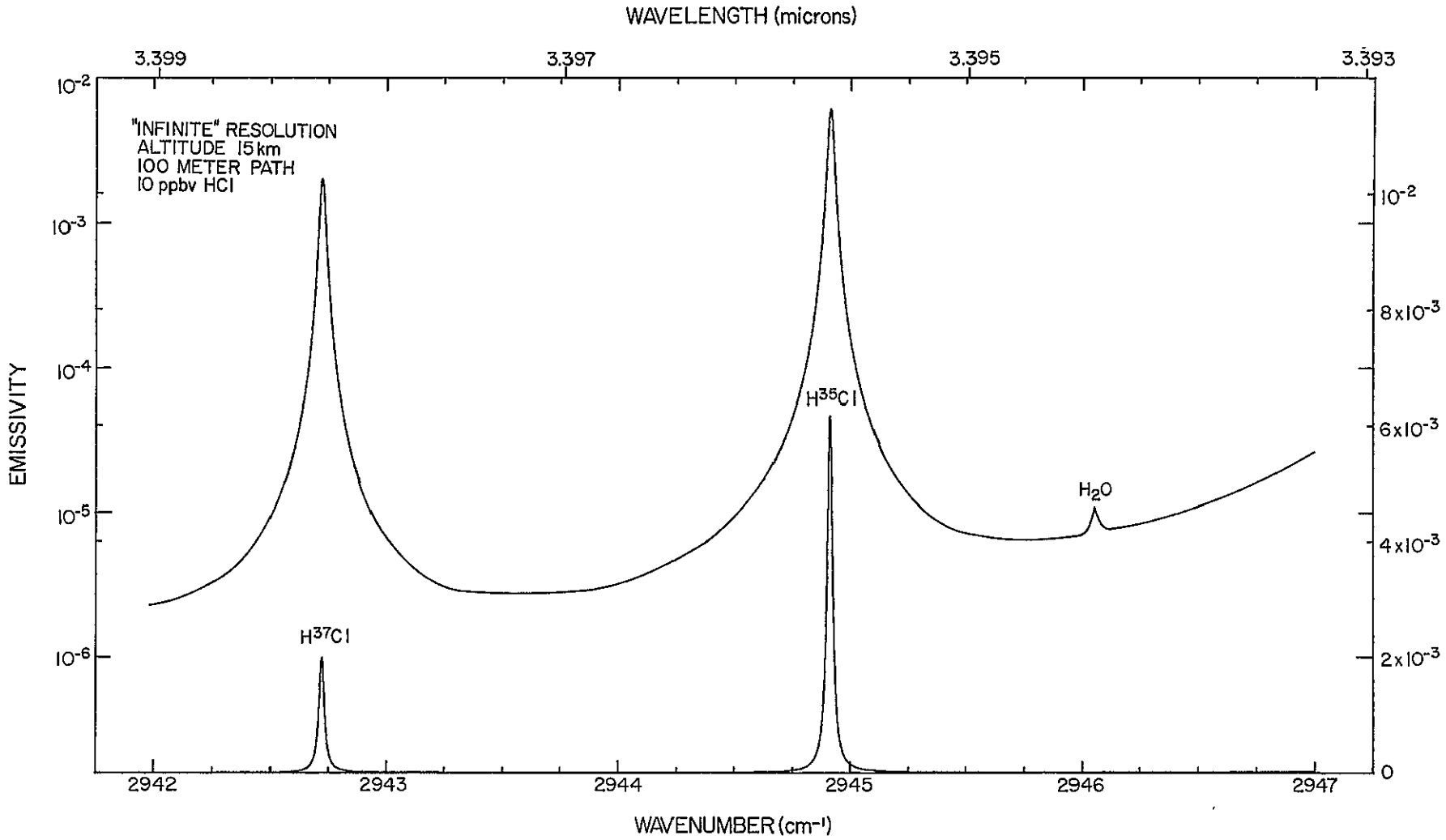
WAVELENGTH (microns)
3.399
3.397
3.395
3.393
"INFINITE" RESOLUTION
ALTITUDE 15 km
100 METER PATH
10 ppbv HCl
H35Cl
H37Cl
H2O
EMISSIVITY
10-2
10-3
10-4
10-5
10-6
8x10-3
6x10-3
4x10-3
2x10-3
0
2942
2943
2944
2945
2946
2947
WAVENUMBER (cm-1)

Figure 9.

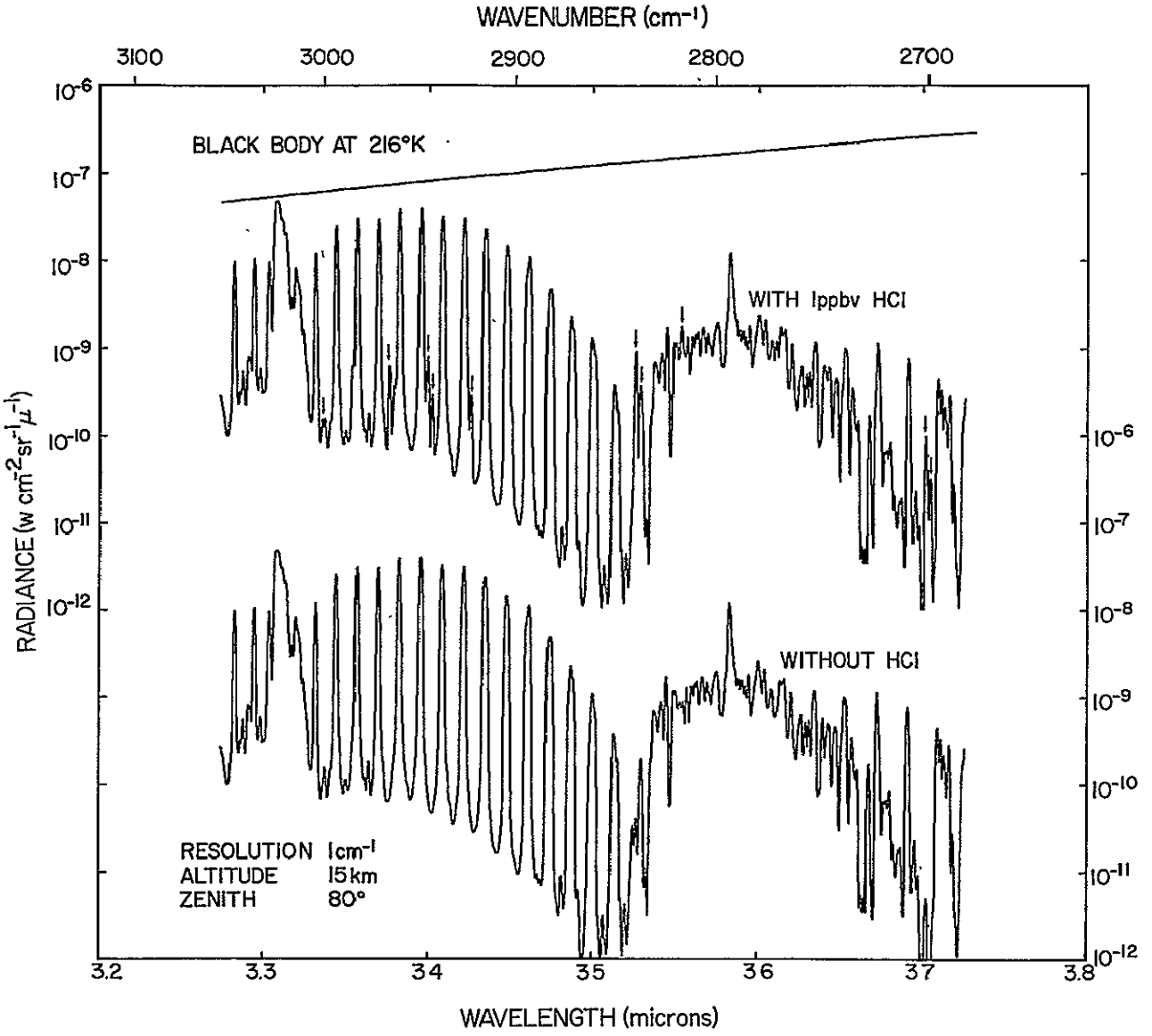
WAVENUMBER (cm⁻¹)
3100
3000
2900
2800
2700
BLACK BODY AT 216°K
WITH 1ppbv HCl
WITHOUT HCl
RESOLUTION 1cm⁻¹
ALTITUDE 15km
ZENITH 80°
RADIANCE (w cm⁻² sr⁻¹ μ⁻¹)
10⁻⁶
10⁻⁷
10⁻⁸
10⁻⁹
10⁻¹⁰
10⁻¹¹
10⁻¹²
3.2
3.3
3.4
3.5
3.6
3.7
3.8
WAVELENGTH (microns)

Figure 10.

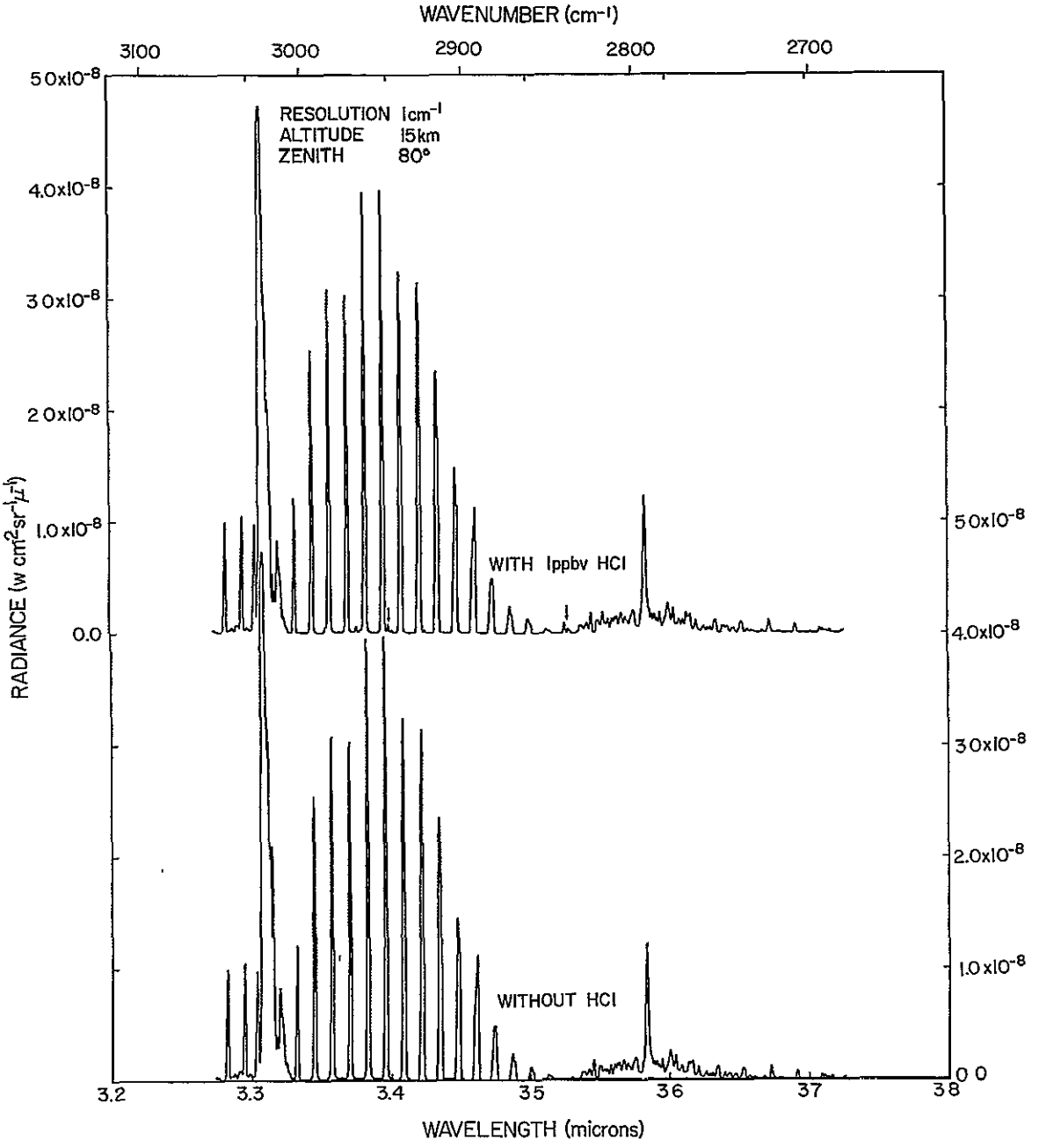
WAVENUMBER (cm⁻¹)
3100
3000
2900
2800
2700
RESOLUTION 1cm⁻¹
ALTITUDE 15km
ZENITH 80°
WITH 1ppbv HCl
WITHOUT HCl
RADIANCE (w cm⁻²sr⁻¹μ⁻¹)
5.0x10⁻⁸
4.0x10⁻⁸
3.0x10⁻⁸
2.0x10⁻⁸
1.0x10⁻⁸
0.0
3.2
3.3
3.4
35
36
37
38
WAVELENGTH (microns)

Figure 11.

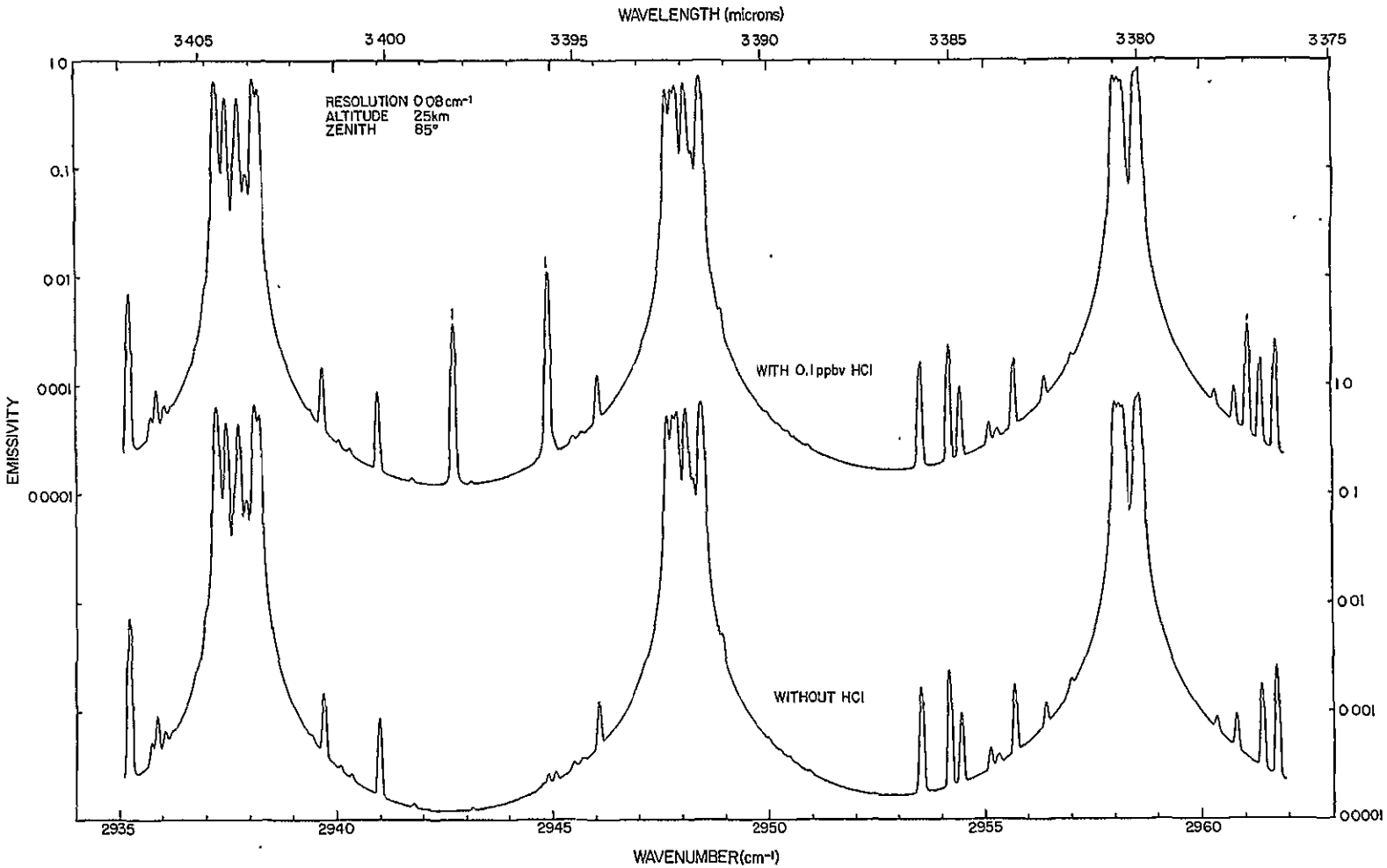
WAVELENGTH (microns)
3405
3400
3395
3390
3385
3380
3375
RESOLUTION 0.08 cm⁻¹
ALTITUDE 25km
ZENITH 85°
WITH 0.1ppbv HCl
WITHOUT HCl
EMISSIVITY
1.0
0.1
0.01
0.001
0.0001
2935
2940
2945
2950
2955
2960
WAVENUMBER(cm⁻¹)

Figure 12.

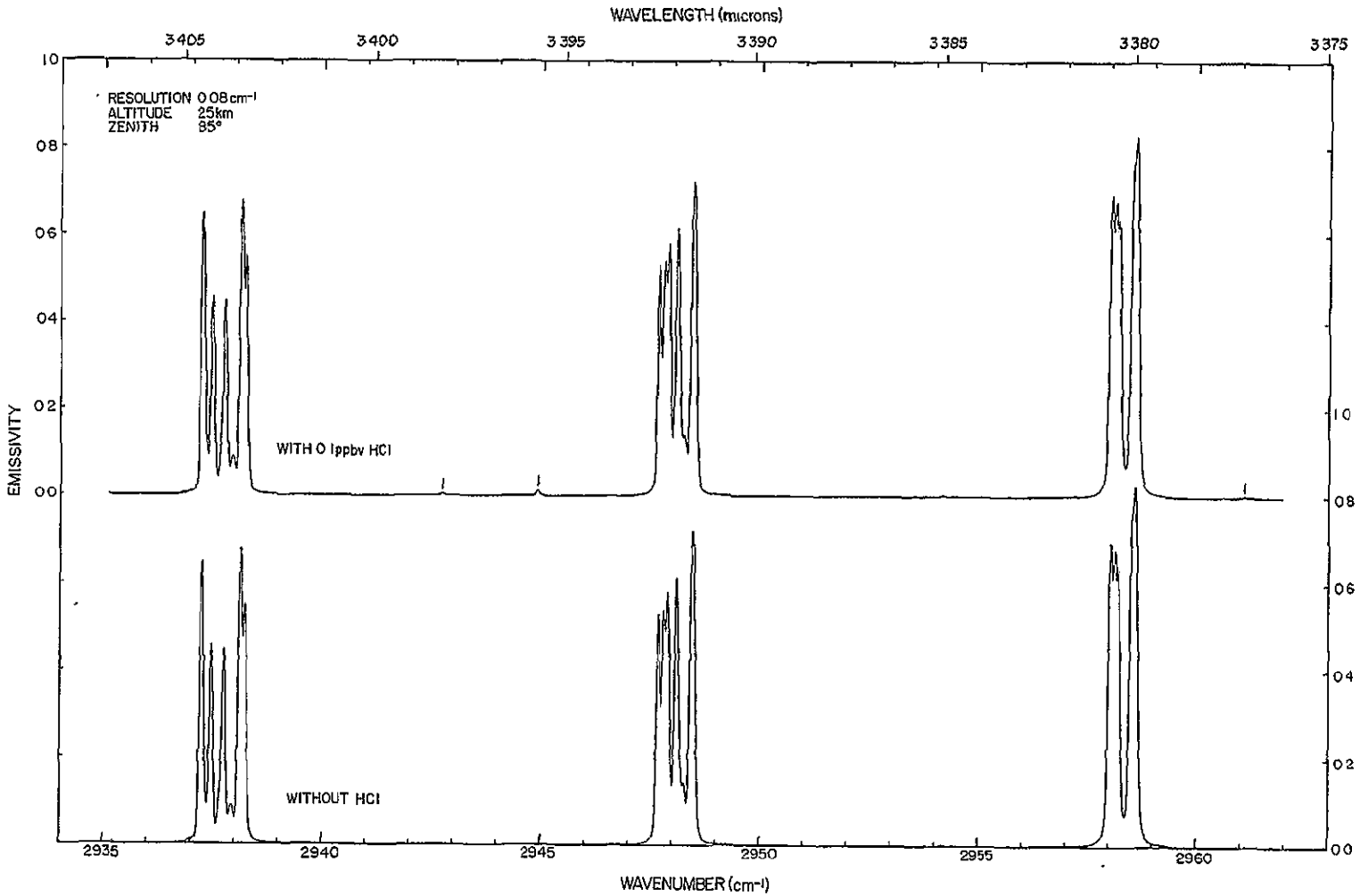
WAVELENGTH (microns)
3405
3400
3395
3390
3385
3380
3375
RESOLUTION 0 08cm-1
ALTITUDE 25km
ZENITH 85°
WITH O 1ppbv HCl
WITHOUT HCl
EMISSIVITY
10
08
06
04
02
00
2935
2940
2945
2950
2955
2960
WAVENUMBER (cm-1)

Figure 13.

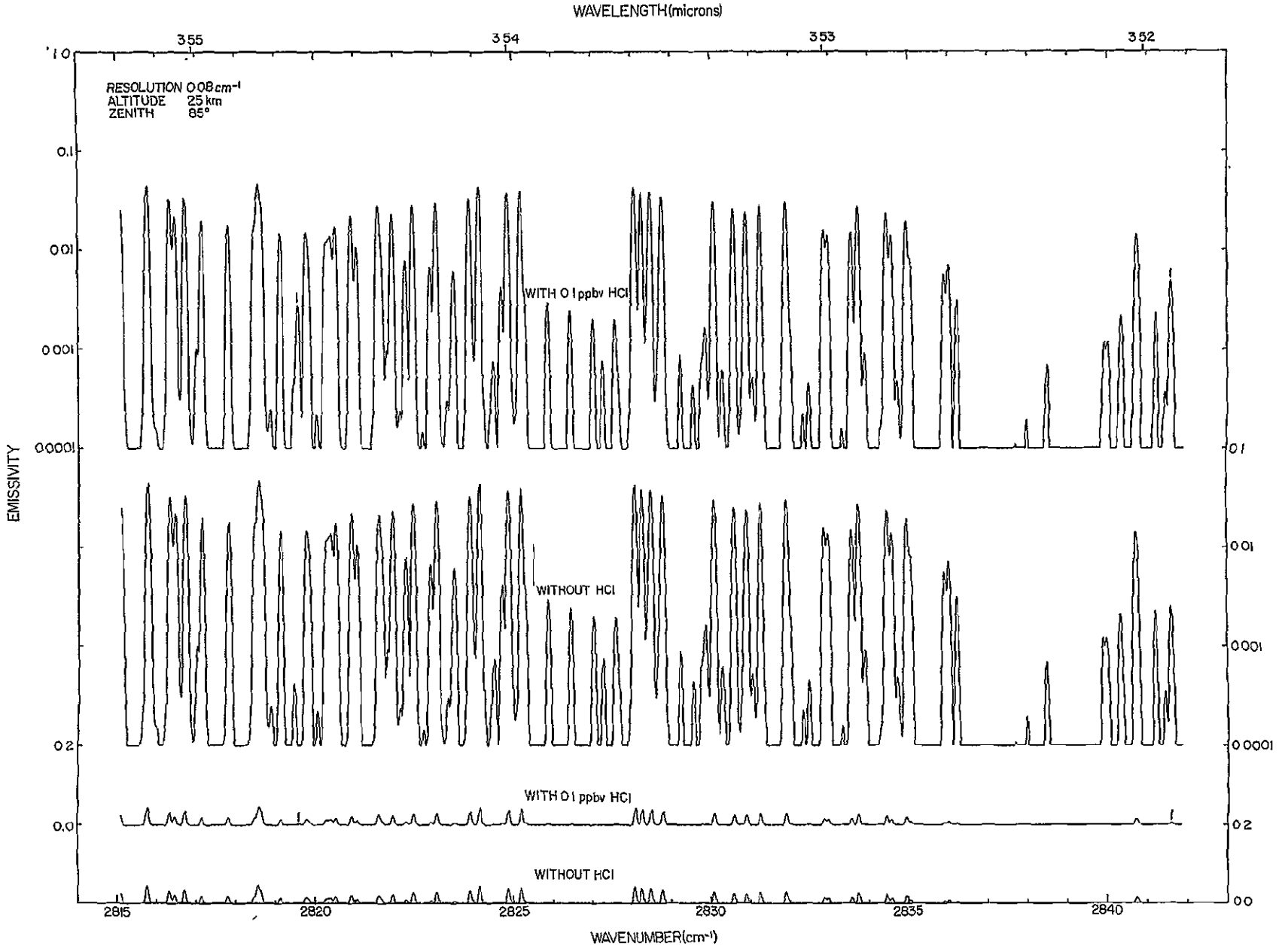
WAVELENGTH(microns)
355
354
353
352
RESOLUTION 0.08 cm⁻¹
ALTITUDE 25 km
ZENITH 85°
1.0
0.1
0.01
0.001
0.0001
EMISSIVITY
WITH 0.1 ppbv HCl
WITHOUT HCl
0.2
0.0
WITH 0.1 ppbv HCl
WITHOUT HCl
0.1
0.01
0.001
0.0001
0.2
0.0
2815
2820
2825
2830
2835
2840
WAVENUMBER(cm⁻¹)

Figure 14.

III. C. HF

The spectral lines in the (0-1) fundamental band of HF are significantly stronger than the (0-1) HCl lines, but in general, the atmospheric interference is stronger in the HF case. The major interferences result from the H_2O and CO_2 2.7μm bands and thus the lower wavelength side of these bands is a more promising region for HF detection.

"Infinite" resolution absorption spectra are calculated for a 100 meter path at 5.5 km altitude in Figure 15. Scaling the figures to ~1% emissivity shows that ~3 ppbv HF should be measurable in the 4039 cm^{-1} region, where the HF line is significantly stronger than the background atmospheric lines, but is not completely isolated.

The effect of adding 0.2 ppbv HF to the atmosphere on the spectral radiance calculated from 15 km, at 80° zenith angle and 1 cm^{-1} resolution is shown in Figures 16 and 17. Several quite isolated HF features are seen to be comparable in intensity to the atmospheric peaks. The radiance levels of ~2×10^{-12} w cm^{-2} sr^{-1} μm^{-1} are marginal for the capability of "state of the art" spectral radiometers.

In terms of atmospheric absorption measurements, Figures 16 and 17 yield ~1% absorptivity. Thus ~0.2 ppbv HF should be measurable in the solar spectrum with currently available solar spectrometers which are capable of better than 0.5 cm^{-1} resolution.

Atmospheric absorptions with and without HF are calculated for solar spectrum measurements from an altitude of 25 km, an 85° zenith angle and 0.08 cm^{-1} resolution (Figure 18). The HF line near 4039 cm^{-1} is well above the atmospheric lines and an ~1% measurable absorptivity permits the measurement of ~0.02 ppbv HF.

The HF line parameters and the atmospheric line parameters are relatively accurate for this region; however, closer attention should be given to the effects of solar lines in solar spectrum measurements.

High-altitude solar spectra in this region under ~1 cm^{-1} resolution[29] show strong solar features between 4020 and 4030 cm^{-1} and much weaker features near the 4039 cm^{-1} HF line.

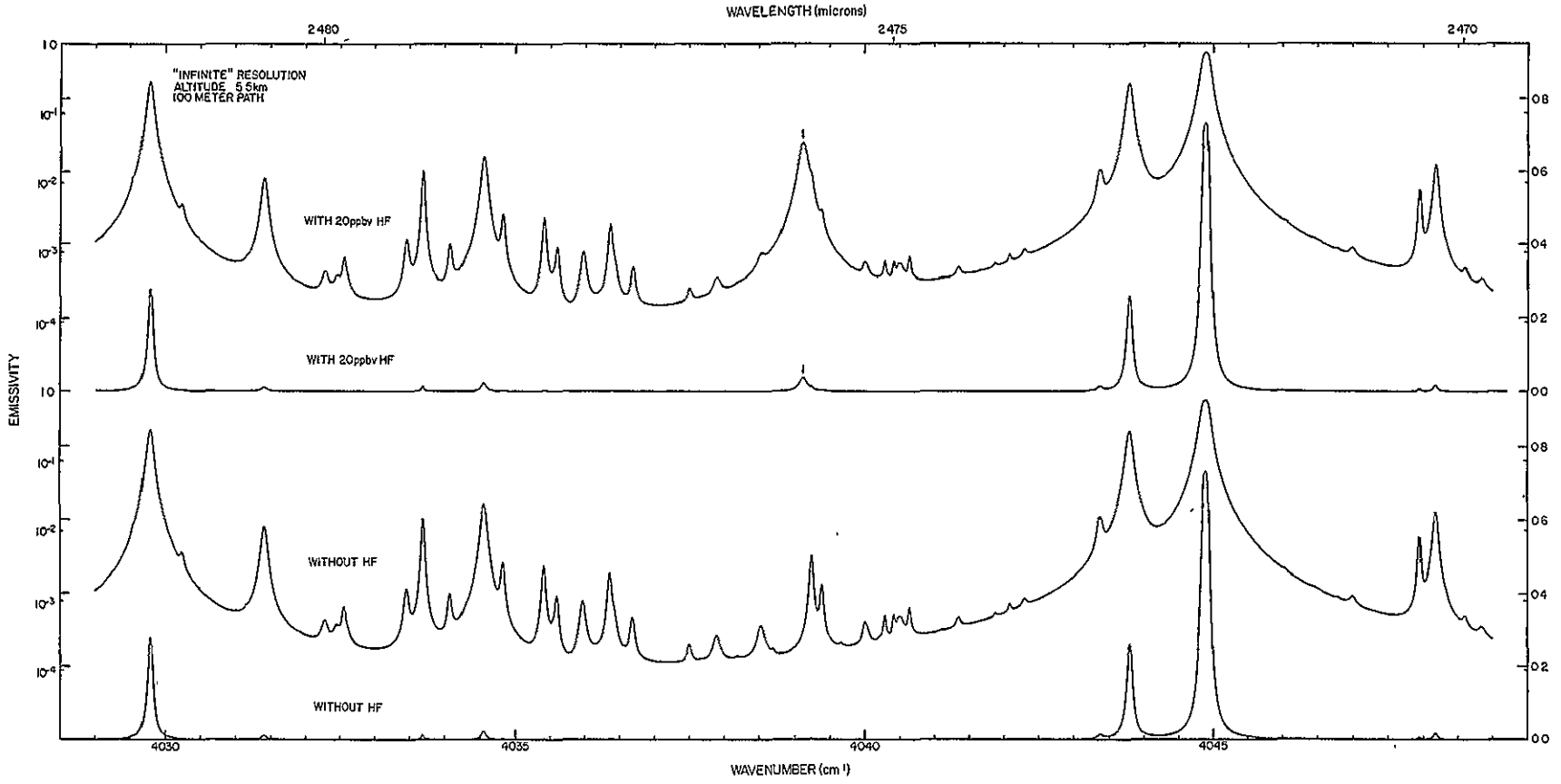
WAVELENGTH (microns)
2480
2475
2470
"INFINITE" RESOLUTION
ALTITUDE 5.5km
100 METER PATH
WITH 20ppbv HF
WITH 20ppbv HF
WITHOUT HF
WITHOUT HF
EMISSIVITY
4030
4035
4040
4045
WAVENUMBER (cm⁻¹)

Figure 15.

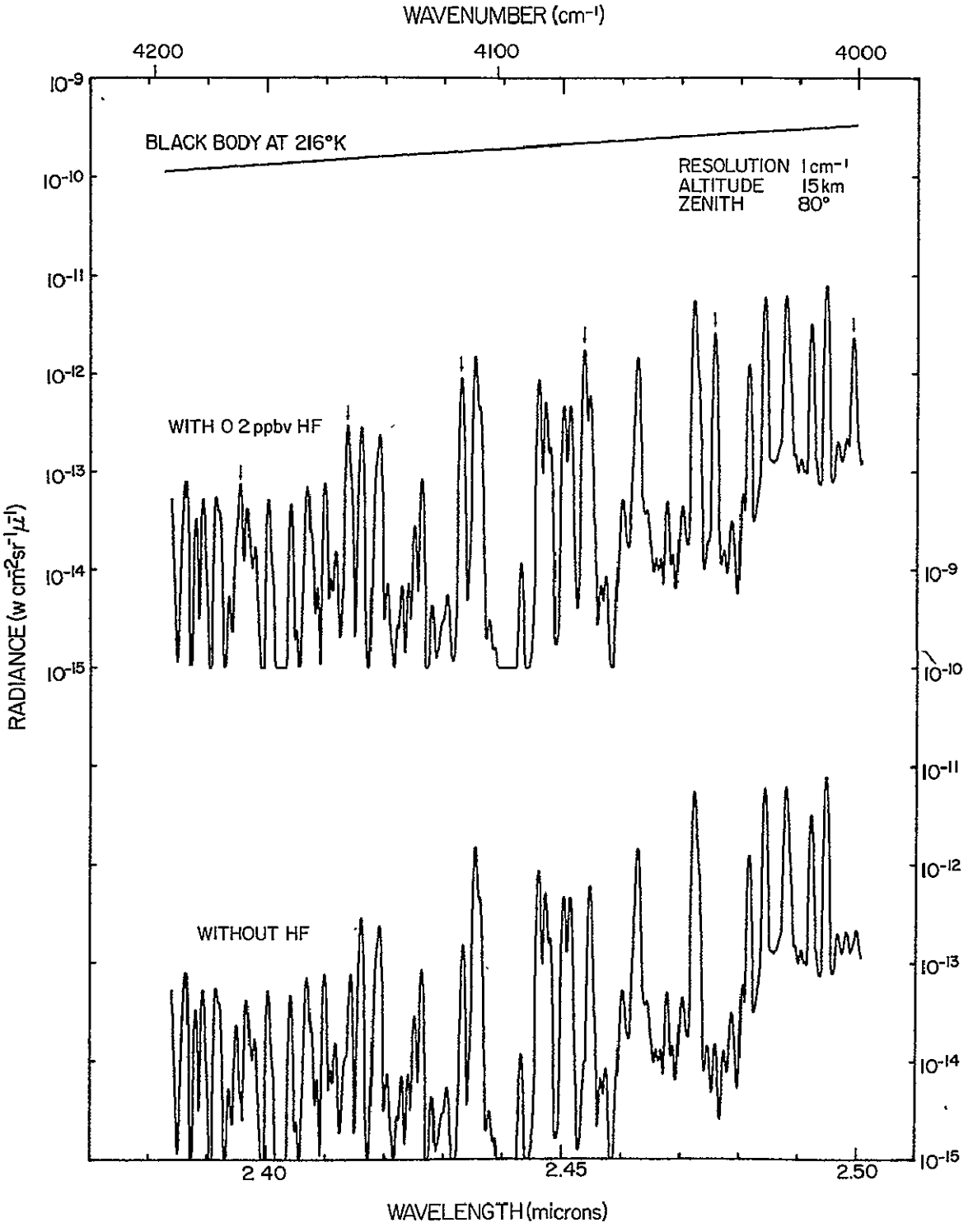
WAVENUMBER (cm⁻¹)
4200
4100
4000
BLACK BODY AT 216°K
RESOLUTION 1 cm⁻¹
ALTITUDE 15 km
ZENITH 80°
WITH 0 2 ppbv HF
WITHOUT HF
RADIANCE (w cm⁻² sr⁻¹ μ⁻¹)
10⁻⁹
10⁻¹⁰
10⁻¹¹
10⁻¹²
10⁻¹³
10⁻¹⁴
10⁻¹⁵
2 40
2.45
2.50
WAVELENGTH (microns)

Figure 16.

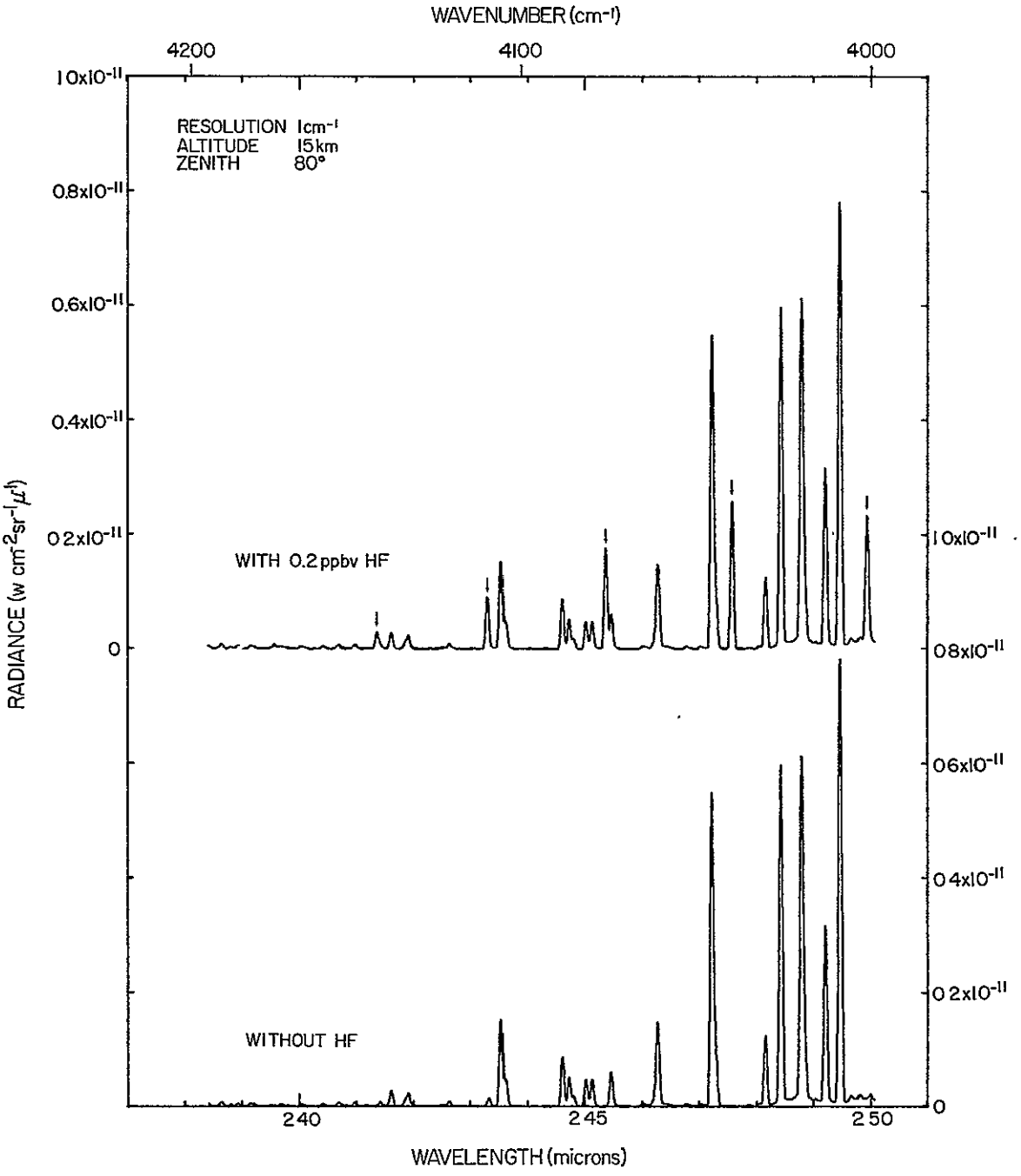
WAVENUMBER (cm⁻¹)
4200
4100
4000
RESOLUTION 1cm⁻¹
ALTITUDE 15km
ZENITH 80°
WITH 0.2ppbv HF
WITHOUT HF
RADIANCE (w cm⁻²sr⁻¹μ⁻¹)
1.0x10⁻¹¹
0.8x10⁻¹¹
0.6x10⁻¹¹
0.4x10⁻¹¹
0.2x10⁻¹¹
0
240
245
250
WAVELENGTH (microns)

Figure 17.

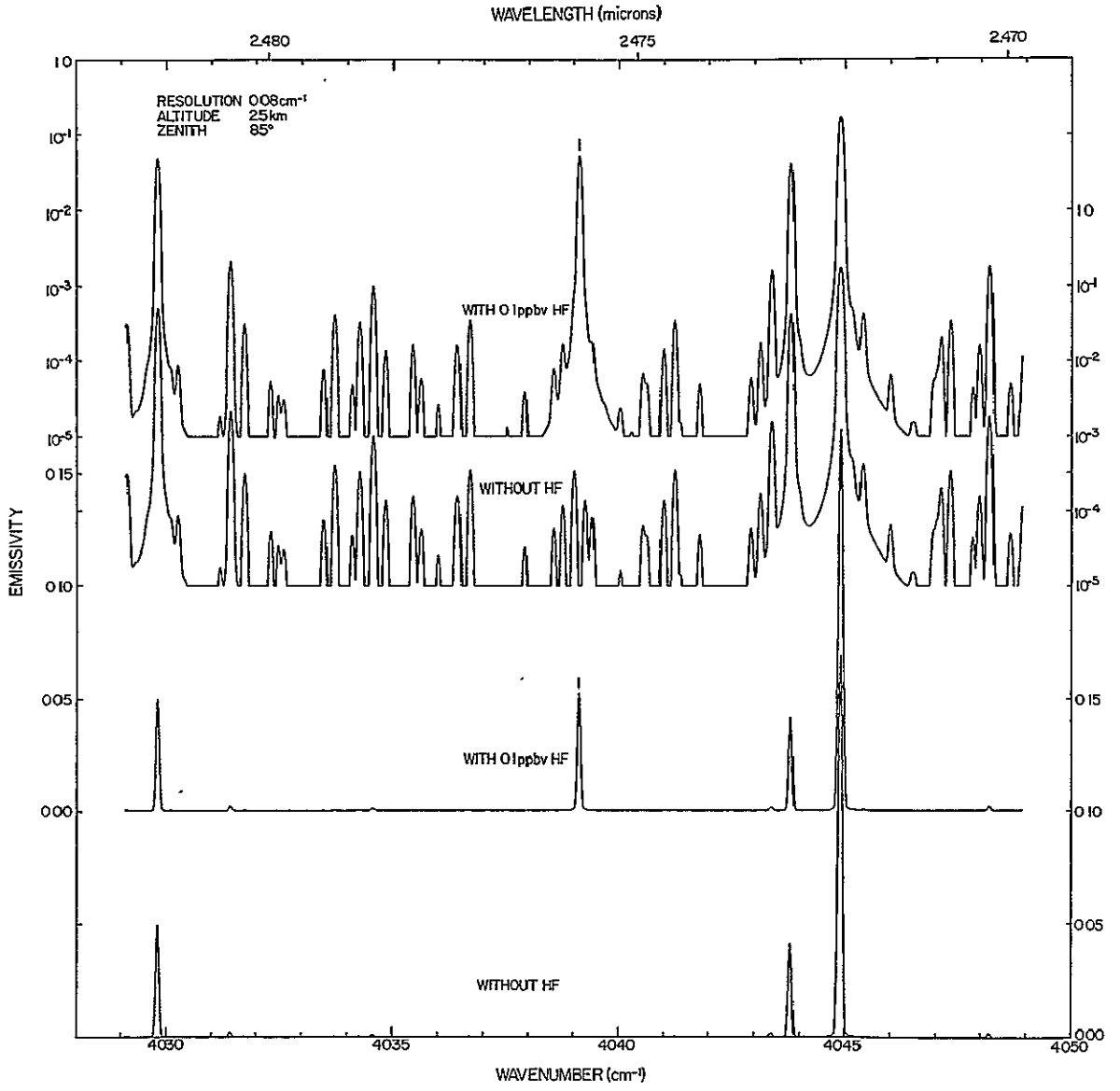
WAVELENGTH (microns)
2.480
2.475
2.470
RESOLUTION 0.08cm⁻¹
ALTITUDE 25km
ZENITH 85°
WITH 0.1ppbv HF
WITHOUT HF
WITH 0.1ppbv HF
WITHOUT HF
EMISSIVITY
1.0
10⁻¹
10⁻²
10⁻³
10⁻⁴
10⁻⁵
0.15
0.10
0.05
0.00
4030
4035
4040
4045
4050
WAVENUMBER (cm⁻¹)

Figure 18.

III. D. HNO_3

A recent paper[40] has summarized the spectral parameters available for the HNO_3 vibration-rotation bands. Line parameters are not yet available, except for a preliminary compilation for the ν_9 band in the 21.8μm region. However the agreement with observed data in this region is not satisfactory yet. Spectral band model parameters are available for the four strong absorption regions at 5.3μm, 7.5μm, 11.3μm and 21.8μm, but these are limited to spectral resolutions of 5 to 10 cm^{-1}.

Under these limitations it is more useful to estimate limits of detectability for HNO_3 from the already published stratospheric absorption and emission HNO_3 spectra. From these spectra it is apparent that 3 of the 4 regions listed above are very effective for HNO_3 measurements.

Atmospheric HNO_3 absorption spectra in the 11.3μm region at ~0.4 cm^{-1} resolution are presented in Figure 2 of Ref. 32. From the upper spectra in this figure it can be estimated that at a 90° zenith angle, 30 km altitude, and resolution of 0.08 cm^{-1}, ~1 ppbv could be measured. The 11.3μm region is the most suitable region for HNO_3 measurements above the troposphere, where the interference with the H_2O and CO_2 lines is quite small. Similar estimates for 90° zenith angle and 30 km altitude can also be derived from the 21.8μm solar spectra, such as those presented in Figures 2 and 3 of Ref. 36, and from the 7.5μm solar spectra presented in Figure 5 of Ref. 32. However the interference with other atmospheric species in the 5.9μm and the 21.8μm region is greater than in the 11.3μm region. The interference in the 5.9μm region (see Figure 8 of Ref. 32) makes this region considerably more difficult for HNO_3 measurements. Figure 9 of Ref. 41 shows atmospheric HNO_3 absorption spectra obtained in the 7.5μm

region at ~0.1 cm^{-1} resolution, 16 km altitude and zenith angles of 85° to 90°. From these spectra it can be estimated that the 7.5μm region at 0.08 cm^{-1} resolution could allow the measurement of ~5 ppbv HNO_3 from solar spectra taken at an 85° zenith angle and 16 km altitude.

Atmospheric HNO_3 emission spectra in the 11.3μm region, with ~5 cm^{-1} resolution, such as those shown in Figure 1 of Ref. 42, are available for various altitudes with a zenith angle of 45°. These yield HNO_3 mixing ratios in the range of 1 to 10 ppbv in the 10 to 30 km altitude range. Higher resolution emission spectra will allow a decrease in the detectability limit linearly and also permit HNO_3 measurements at lower altitudes where the interference with H_2O and CO_2 lines is significant. Similar estimates can be made on the basis of the 21.8μm atmospheric spectra such as those presented in Figure 5 of Ref. 36.

III. E. NH_3

The strong ν_2 fundamental band of NH_3 extends over a wide spectral region from ~700 to ~1300 cm^{-1}. However, many of its strong peaks occur in the strong ν_3 ozone band and will be completely masked in the lower stratosphere between 980 and 1070 cm^{-1}. Therefore two spectral regions, on both sides of the ozone bands, were selected for the present study.

Atmospheric spectral radiance calculated with and without NH_3 at these spectral regions for 15 km, an 80° zenith angle and 1 cm^{-1} resolution, are shown in Figures 19-22. A number of measurable NH_3 features can be seen in the 10.3 to 12.4μm region (Figures 19 and 20) with 0.1 ppbv NH_3. The radiance levels are above 10^{-7} w cm^{-2} sr^{-1} μm^{-1}, well within the capability of current spectral radiometers. Figures 21 and 22 cover the 7.9 to 9.3μm region where the many interfering background lines require larger minimum detectable amounts of NH_3. Also, uncertainties are apparent with regard to the 8.6μm N_2O band in this region.

It should be noted that while the atmospheric H_2O and CO_2 line parameters, as well as the NH_3 line parameters in the 9-12μm region, are relatively accurate, the 11.3μm HNO_3 band was not included in the present calculation. However, the HNO_3 features are much broader and thus would allow observation of the NH_3 peaks superimposed on the HNO_3 spectra. The interference of NH_3 lines with both the CO_2 and HNO_3 lines are minimal near 930 cm^{-1}, (see also Ref. 32) which is thus a promising region for NH_3 detection.

The interference effects are further reduced on absorption spectra calculated for solar spectrum measurements from an altitude

of 25 km, an 85° zenith angle and 0.08 cm^{-1} resolution (Figure 23). Here a number of isolated NH_3 peaks make it feasible to measure ~0.05 ppbv NH_3. The interference effects are similar for solar spectrum measurements under similar resolution and zenith angles from an altitude of 35 km, as is shown in Figure 24. However, the optical path is reduced in this case and thus requires a larger proportion of NH_3 for its spectral features to become evident.

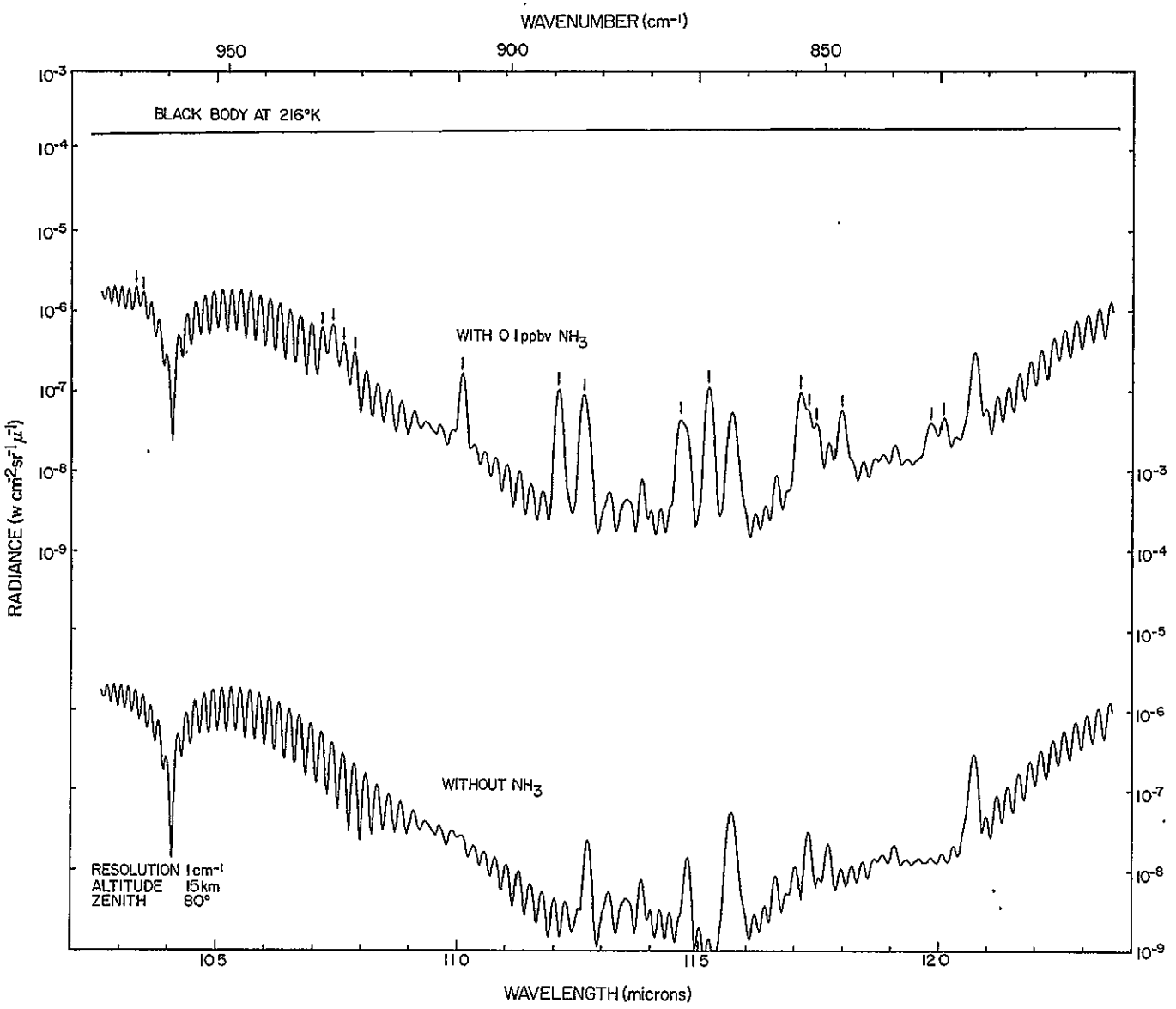
WAVENUMBER (cm⁻¹)
950
900
850
BLACK BODY AT 216°K
WITH O 1ppbv NH3
WITHOUT NH3
RESOLUTION 1cm⁻¹
ALTITUDE 15km
ZENITH 80°
RADIANCE (w cm⁻² sr⁻¹ μ⁻¹)
WAVELENGTH (microns)
105
110
115
120

Figure 19.

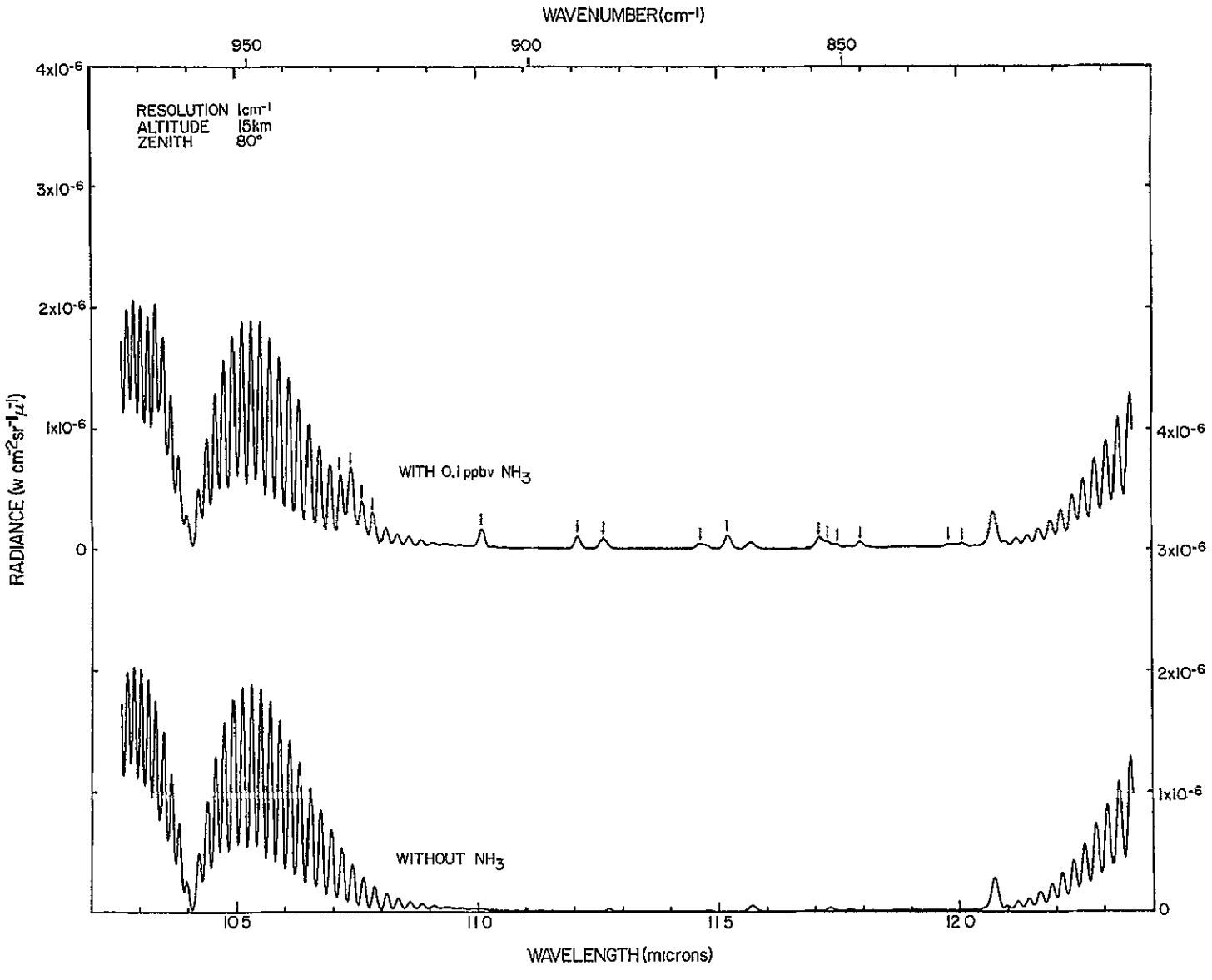
WAVENUMBER(cm-1)
950
900
850
4x10-6
3x10-6
2x10-6
1x10-6
0
RESOLUTION 1cm-1
ALTITUDE 15km
ZENITH 80°
WITH 0.1ppbv NH3
WITHOUT NH3
RADIANCE (w cm-2sr-1μ-1)
105
110
115
120
WAVELENGTH (microns)

Figure 20.

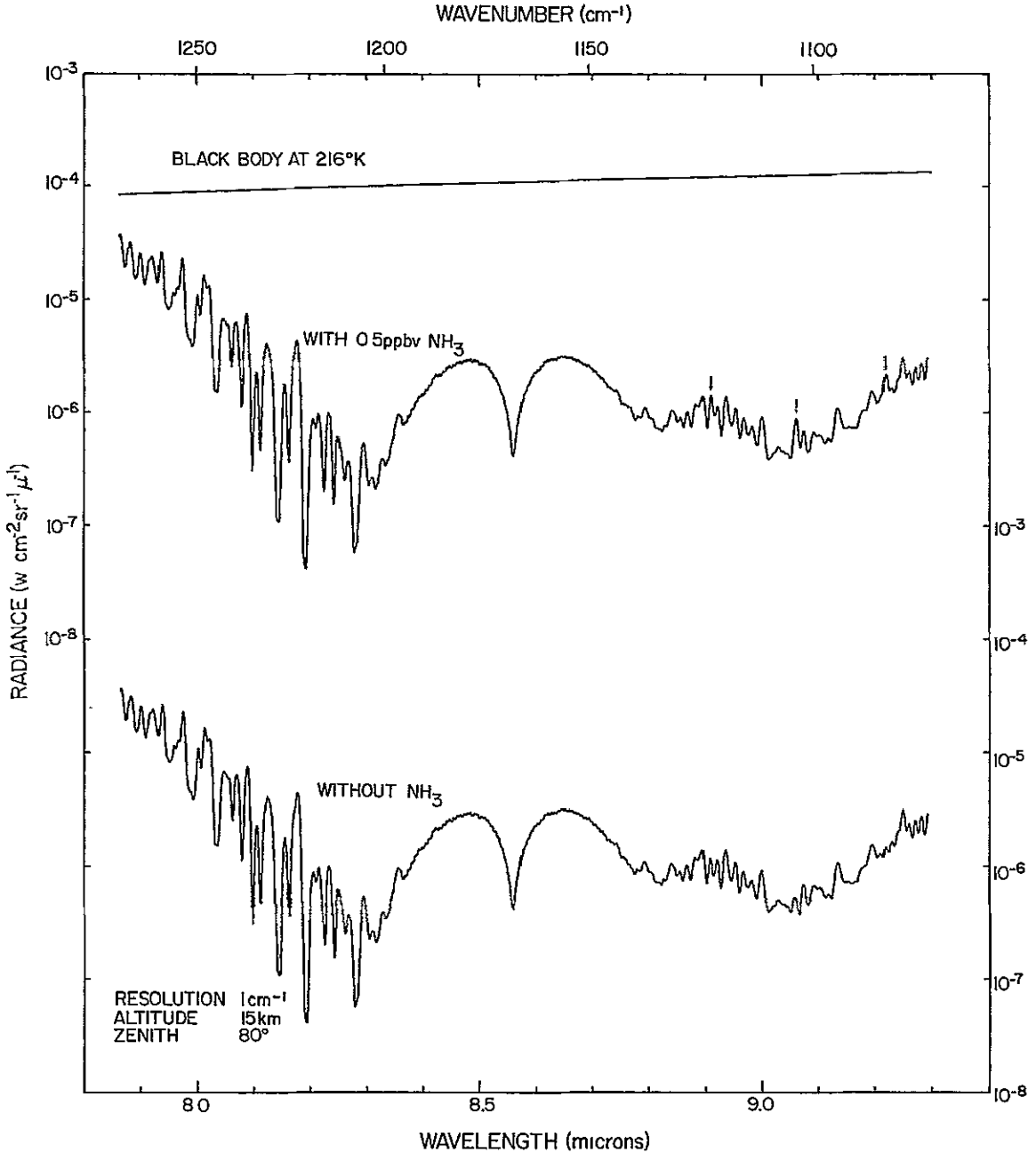
WAVENUMBER (cm⁻¹)
1250
1200
1150
1100
BLACK BODY AT 216°K
WITH 0 5ppbv NH3
WITHOUT NH3
RESOLUTION 1cm⁻¹
ALTITUDE 15km
ZENITH 80°
RADIANCE (w cm⁻²sr⁻¹μ⁻¹)
10⁻³
10⁻⁴
10⁻⁵
10⁻⁶
10⁻⁷
10⁻⁸
8.0
8.5
9.0
WAVELENGTH (microns)

Figure 21.

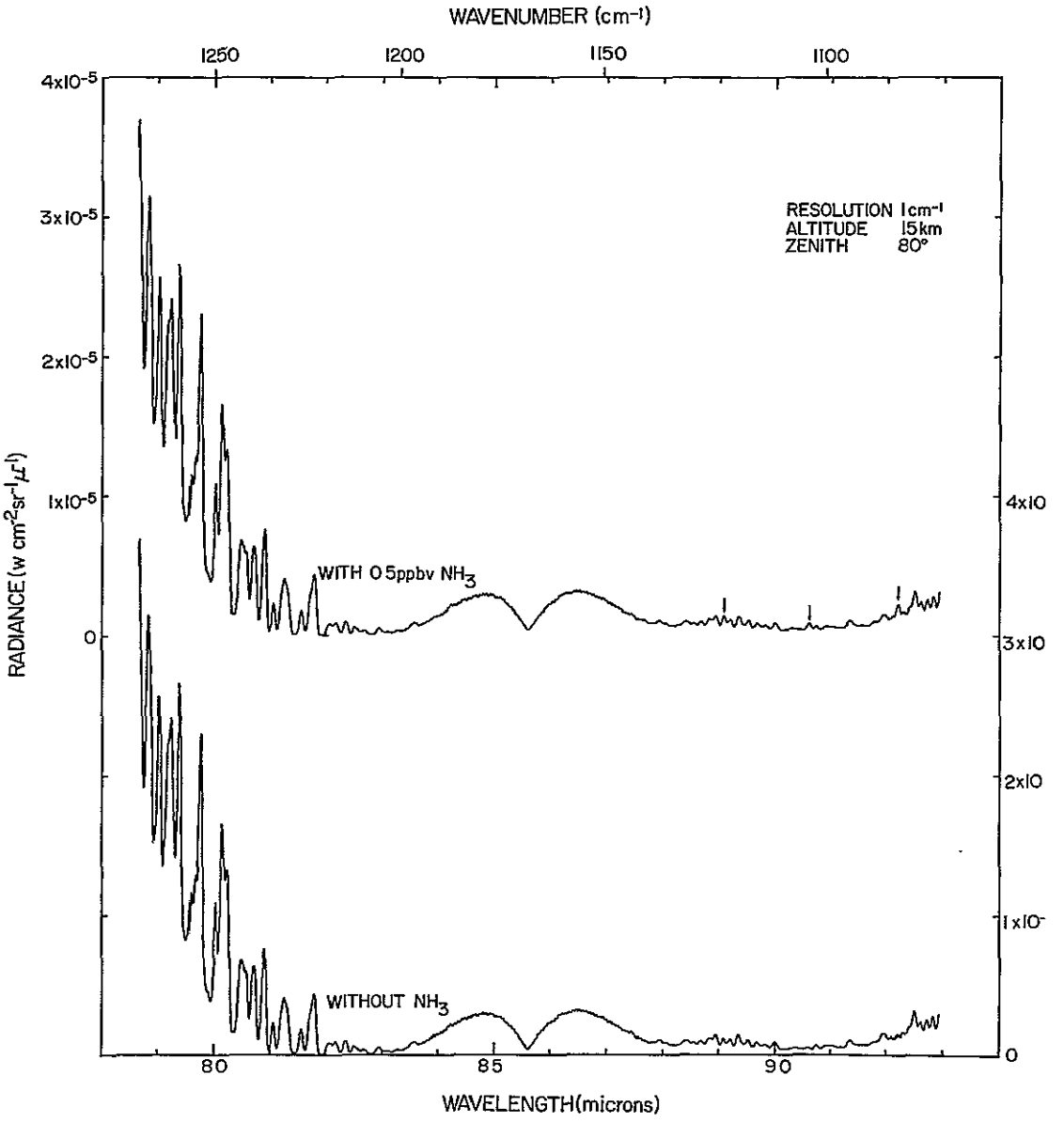
WAVENUMBER (cm⁻¹)
1250
1200
1150
1100
4x10⁻⁵
3x10⁻⁵
2x10⁻⁵
1x10⁻⁵
0
RADIANCE (w cm⁻²sr⁻¹μ⁻¹)
RESOLUTION 1cm⁻¹
ALTITUDE 15km
ZENITH 80°
WITH 0 5ppbv NH3
WITHOUT NH3
4x10
3x10
2x10
1x10⁻
0
80
85
90
WAVELENGTH(microns)

Figure 22.

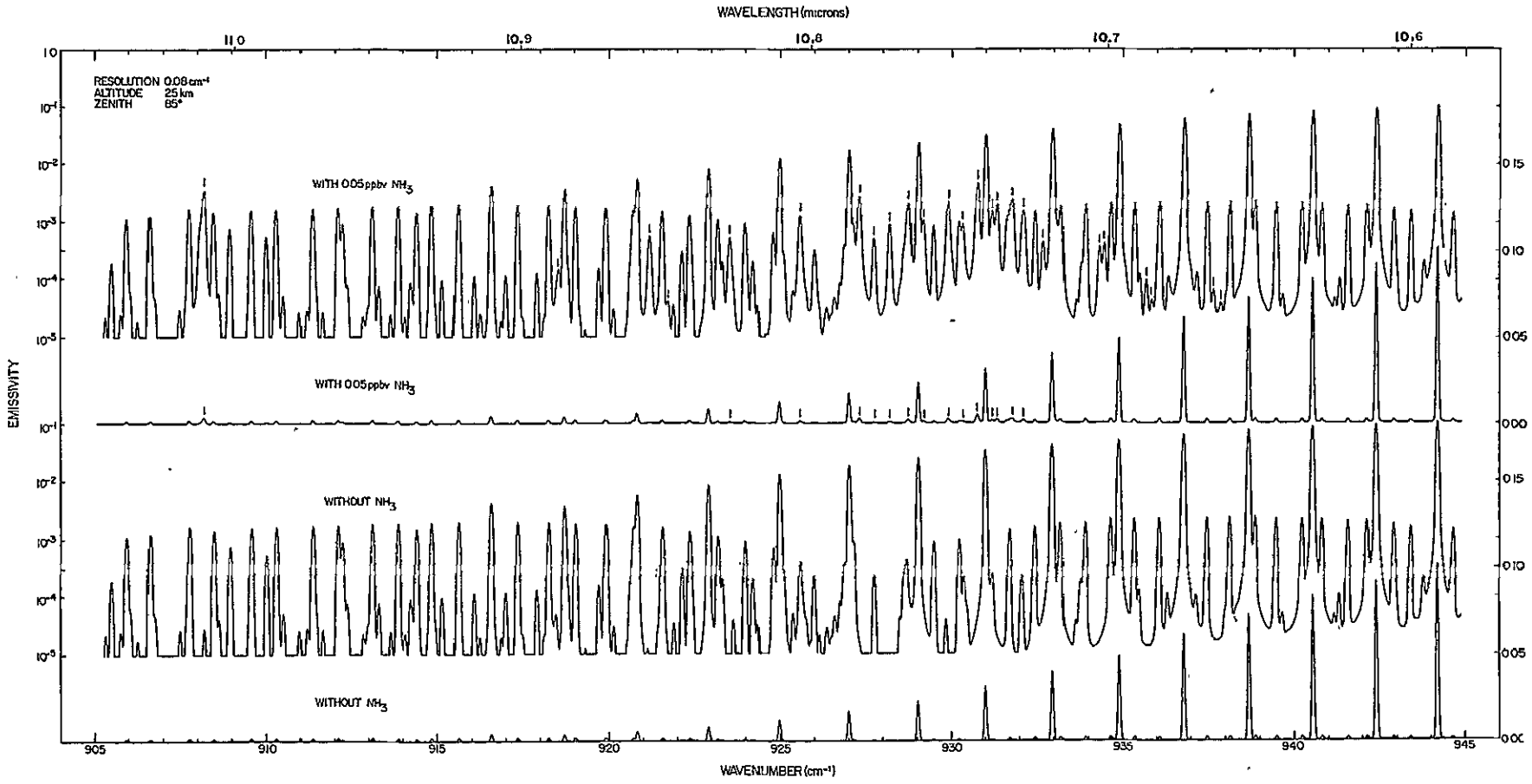
WAVELENGTH (microns)
11.0
10.9
10.8
10.7
10.6
RESOLUTION 0.08 cm⁻¹
ALTITUDE 25 km
ZENITH 85°
WITH 0.05 ppbv NH3
WITH 0.05 ppbv NH3
WITHOUT NH3
WITHOUT NH3
EMISSIVITY
905
910
915
920
925
930
935
940
945
WAVENUMBER (cm⁻¹)

Figure 23.

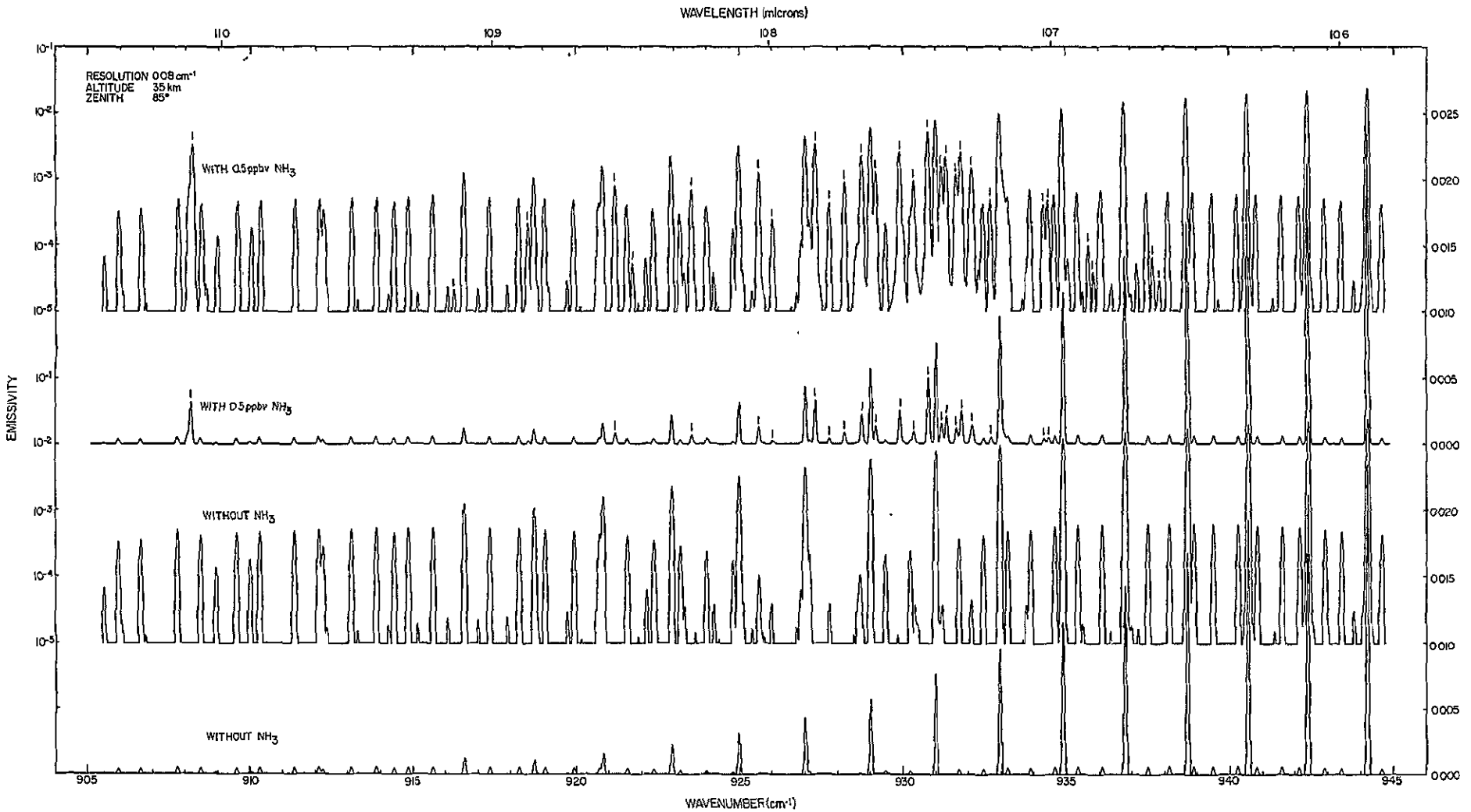
WAVELENGTH (microns)
110
109
108
107
106
RESOLUTION 0.08 cm⁻¹
ALTITUDE 35 km
ZENITH 85°
WITH 0.5ppbv NH3
WITH 0.5ppbv NH3
WITHOUT NH3
WITHOUT NH3
EMISSIVITY
10⁻¹
10⁻²
10⁻³
10⁻⁴
10⁻⁵
0.025
0.020
0.015
0.010
0.005
0.000
905
910
915
920
925
930
935
940
945
WAVENUMBER (cm⁻¹)

Figure 24.

III.F. NO

A detailed study of possible NO absorption measurements from the solar spectrum as observed from various altitudes has been presented previously.[19] Additional emission and absorption spectra are calculated here.

Atmospheric emission spectra are calculated for a spectral radiometer at an altitude of 15 km, an 80^{o} zenith angle and 0.8 cm^{-1} resolution in Figures 25 and 26. It is seen that the NO lines overlap with numerous atmospheric lines. The addition of 5 ppbv NO results in several marginally measurable NO features, but none of the NO features is completely isolated from atmospheric lines. The radiance levels are of the order of 10^{-7} w cm^{-2} sr^{-1} μm^{-1} and are within the capability of "state of the art" spectral radiometers. The absorptivities of the NO features shown in Figures 25 and 26 are of the order of ~1%, but do not include the solar CO features.[19]

"Infinite" resolution absorption spectra are calculated in Figure 27 for a 100 meter path at 15 km altitude. The atmospheric interference is significantly reduced under these conditions and many of the NO features are quite isolated. However, the optical path is considerably smaller so that the ~1% absorptivity criterion permits the measurement of ~50 ppbv NO (by scaling Figure 27).

It should be noted that while the NO line parameters are relatively accurate, the accuracy of many of the atmospheric line parameters in the NO region is significantly less, especially for the weak CO_2 lines.[19] In addition, the solar CO effects, as presented previously[19] should be taken into account.

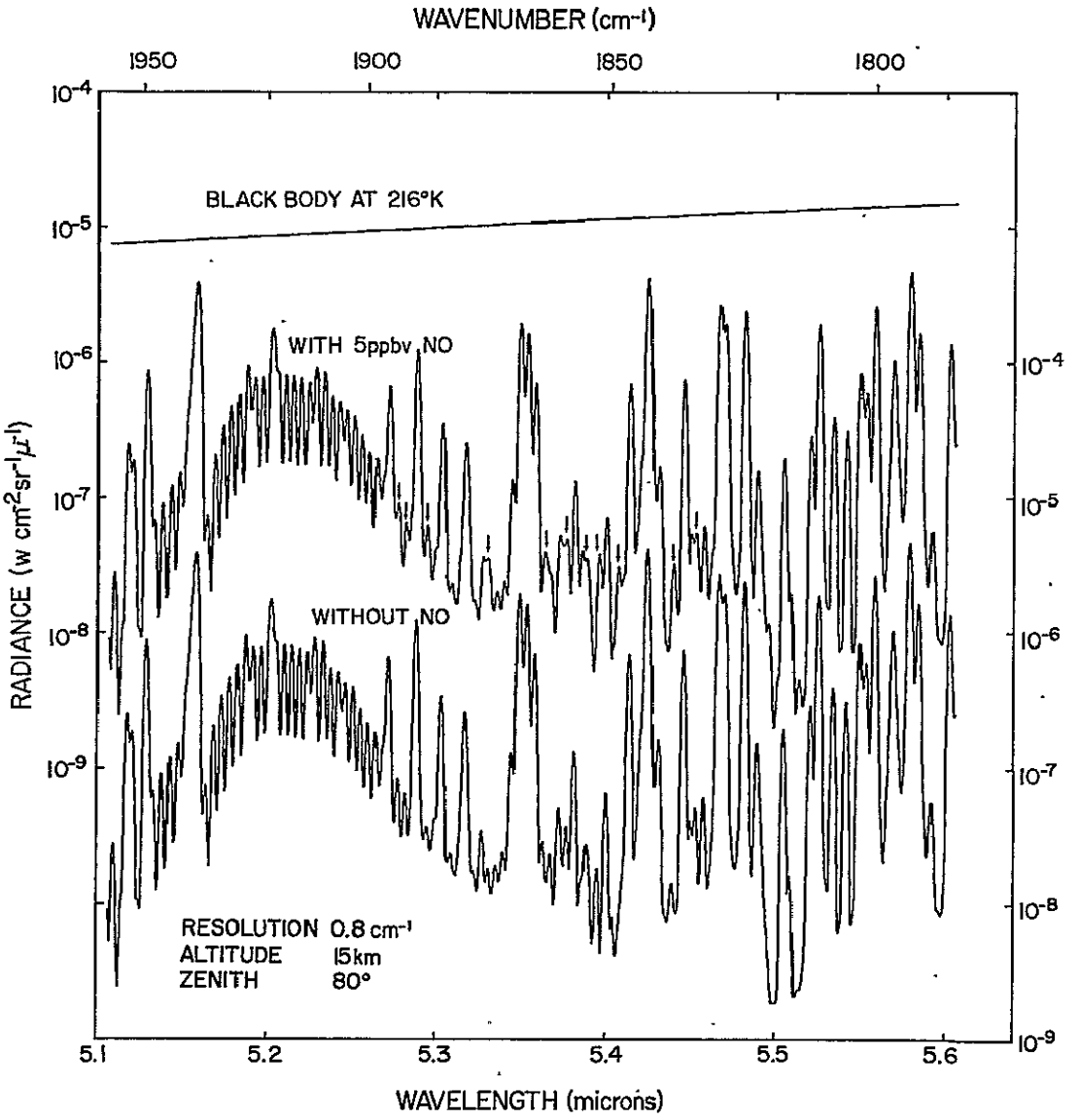
WAVENUMBER (cm⁻¹)
1950
1900
1850
1800
BLACK BODY AT 216°K
WITH 5ppbv NO
WITHOUT NO
RESOLUTION 0.8 cm⁻¹
ALTITUDE 15km
ZENITH 80°
RADIANCE (w cm⁻²sr⁻¹μ⁻¹)
10⁻⁴
10⁻⁵
10⁻⁶
10⁻⁷
10⁻⁸
10⁻⁹
5.1
5.2
5.3
5.4
5.5
5.6
WAVELENGTH (microns)

Figure 25.

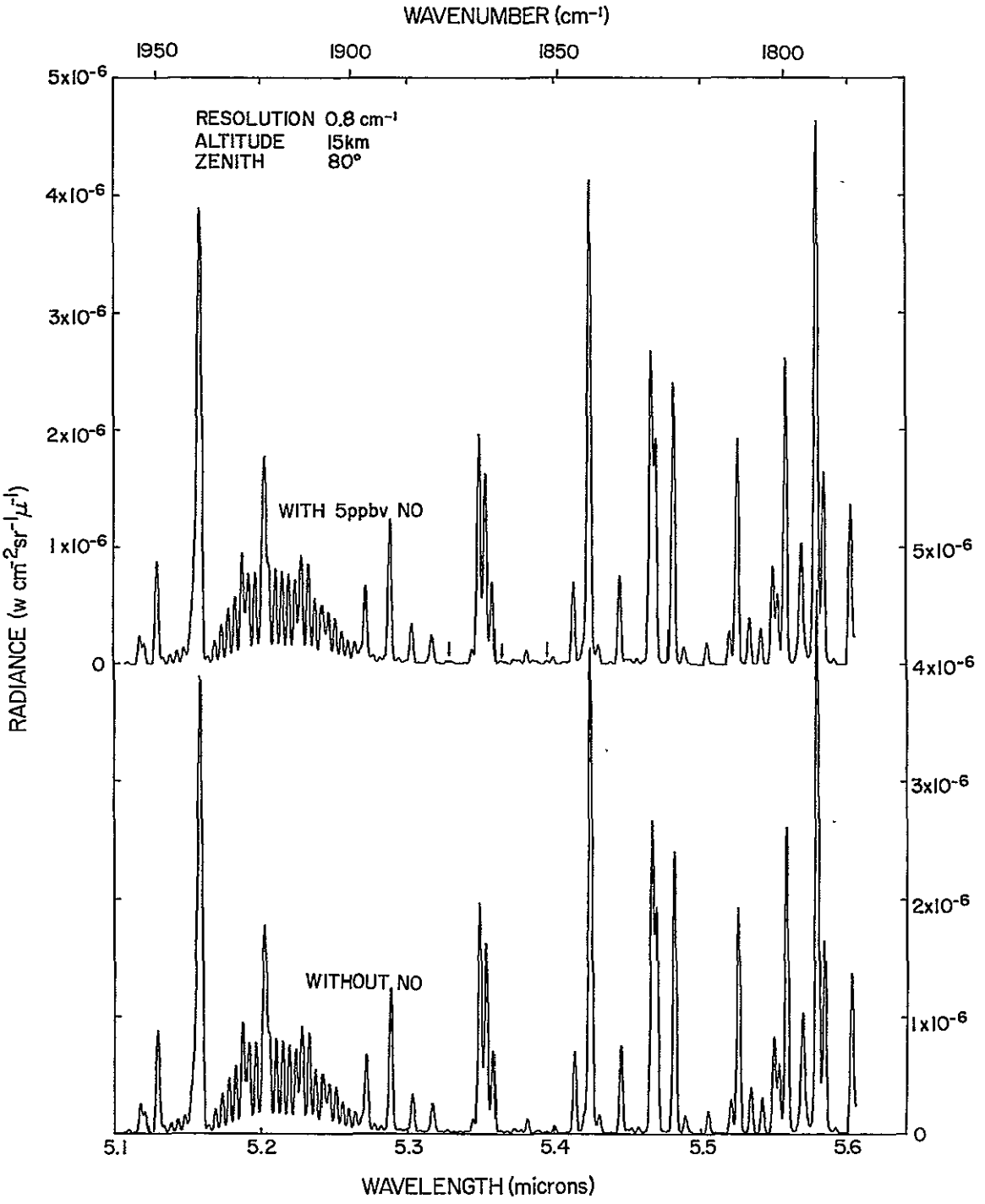
WAVENUMBER (cm⁻¹)
1950
1900
1850
1800
RESOLUTION 0.8 cm⁻¹
ALTITUDE 15km
ZENITH 80°
WITH 5ppbv NO
WITHOUT NO
RADIANCE (w cm⁻²sr⁻¹μ⁻¹)
5x10⁻⁶
4x10⁻⁶
3x10⁻⁶
2x10⁻⁶
1x10⁻⁶
0
5.1
5.2
5.3
5.4
5.5
5.6
WAVELENGTH (microns)

Figure 26.

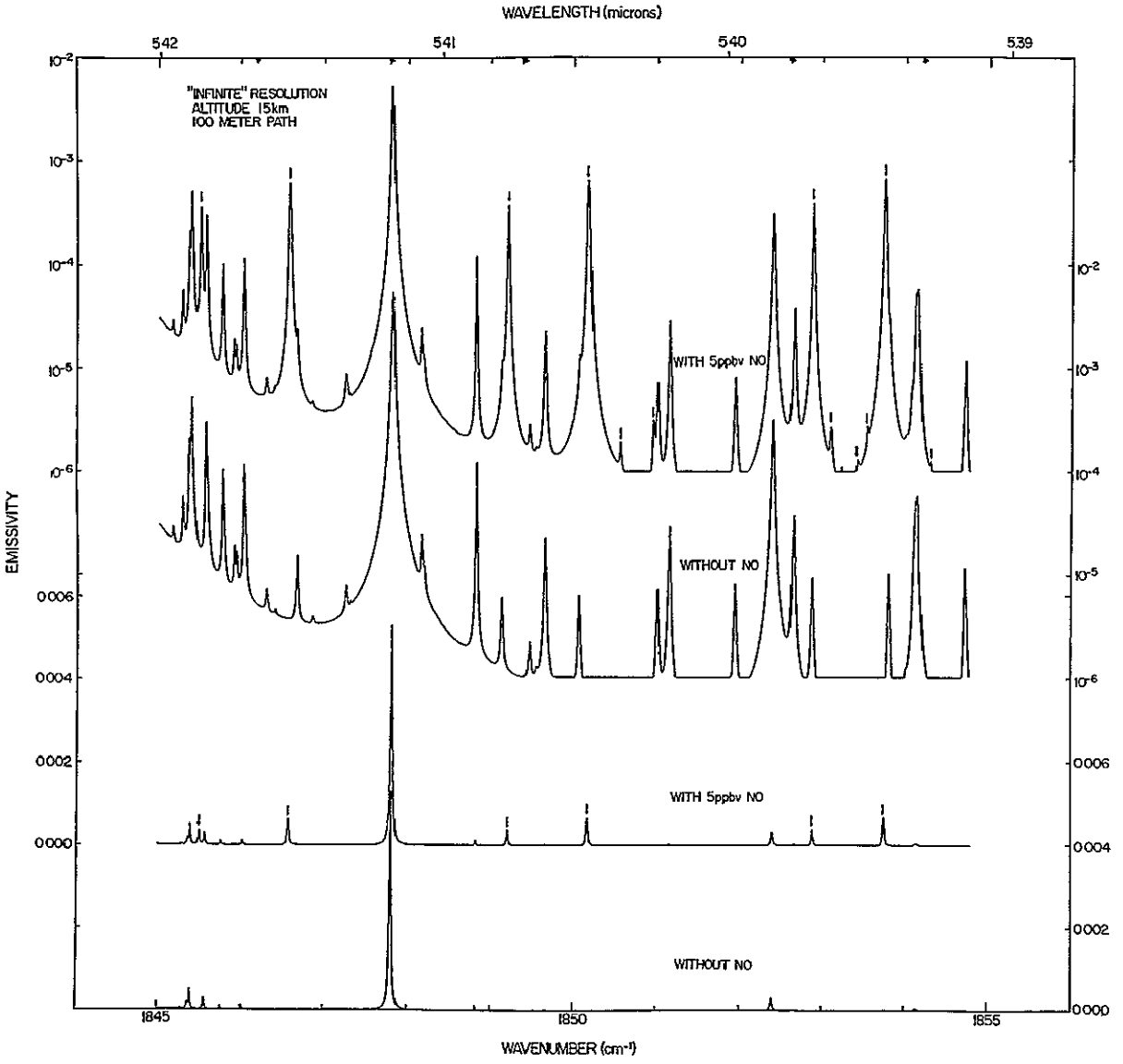
WAVELENGTH (microns)
542
541
540
539
"INFINITE" RESOLUTION
ALTITUDE 15km
100 METER PATH
WITH 5ppbv NO
WITHOUT NO
WITH 5ppbv NO
WITHOUT NO
EMISSIVITY
1845
1850
1855
WAVENUMBER (cm⁻¹)

Figure 27.

III. G. NO_2

The ν_3 band of NO_2 is the strongest of the NO_2 bands. However this band occurs near the center of the strong 6.3μm H_2O band so that the determination of NO_2 from low resolution, long path measurements at low altitudes would be impractical. The masking effect of the numerous atmospheric lines on the NO_2 lines is significantly reduced when higher spectral resolution and higher altitudes are used, thereby making measurements feasible.

Atmospheric absorption calculations, with and without NO_2, are shown in Figures 28 and 29 for a solar spectrum measurement from 25 km altitude, an 85^o zenith angle, and 0.08 cm^{-1} resolution. It is seen that ~1% absorptivity permits the measurement of ~0.1 ppbv NO_2 under these conditions. Many NO_2 lines are clearly isolated from the atmospheric lines, especially near 1605 cm^{-1} where a strong NO_2 line group occurs in an atmospheric "window." Several isolated NO_2 line groups also occur between H_2O lines near 1612 cm^{-1}.

Similar calculations for 35 km are shown in Figure 30. It is apparent that ~1 ppbv NO_2 should be measurable from many isolated lines of NO_2 with an absorptivity of ~1%.

The H_2O line parameters are known to relatively high accuracy in the NO_2 region. However, uncertainties exist with regard to the CH_4 lines in this region and also the NO_2 lines used here.[26]

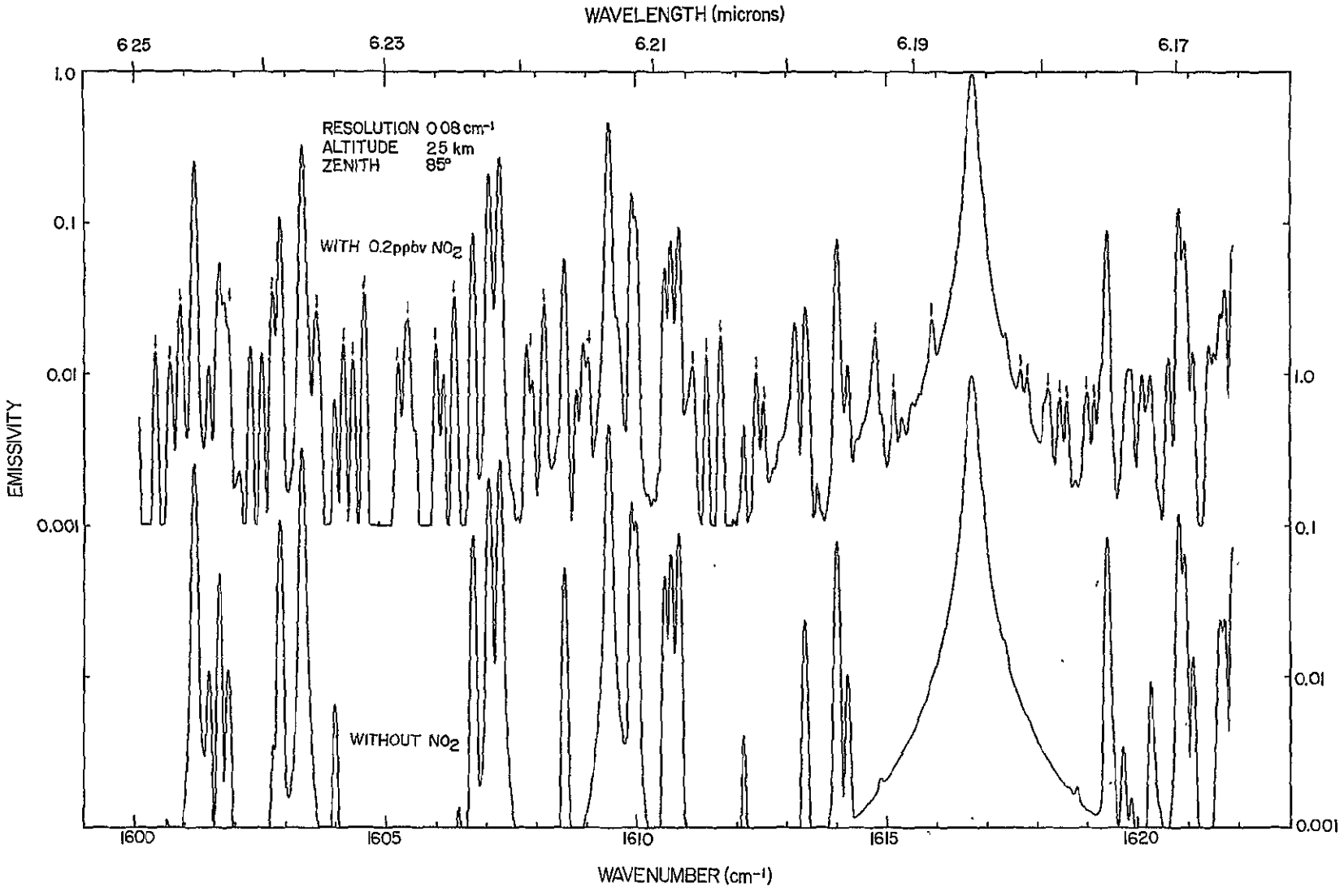
WAVELENGTH (microns)
6.25
6.23
6.21
6.19
6.17
1.0
0.1
0.01
0.001
EMISSIVITY
RESOLUTION 0.08 cm⁻¹
ALTITUDE 25 km
ZENITH 85°
WITH 0.2ppbv NO2
WITHOUT NO2
1600
1605
1610
1615
1620
WAVENUMBER (cm⁻¹)

Figure 28.

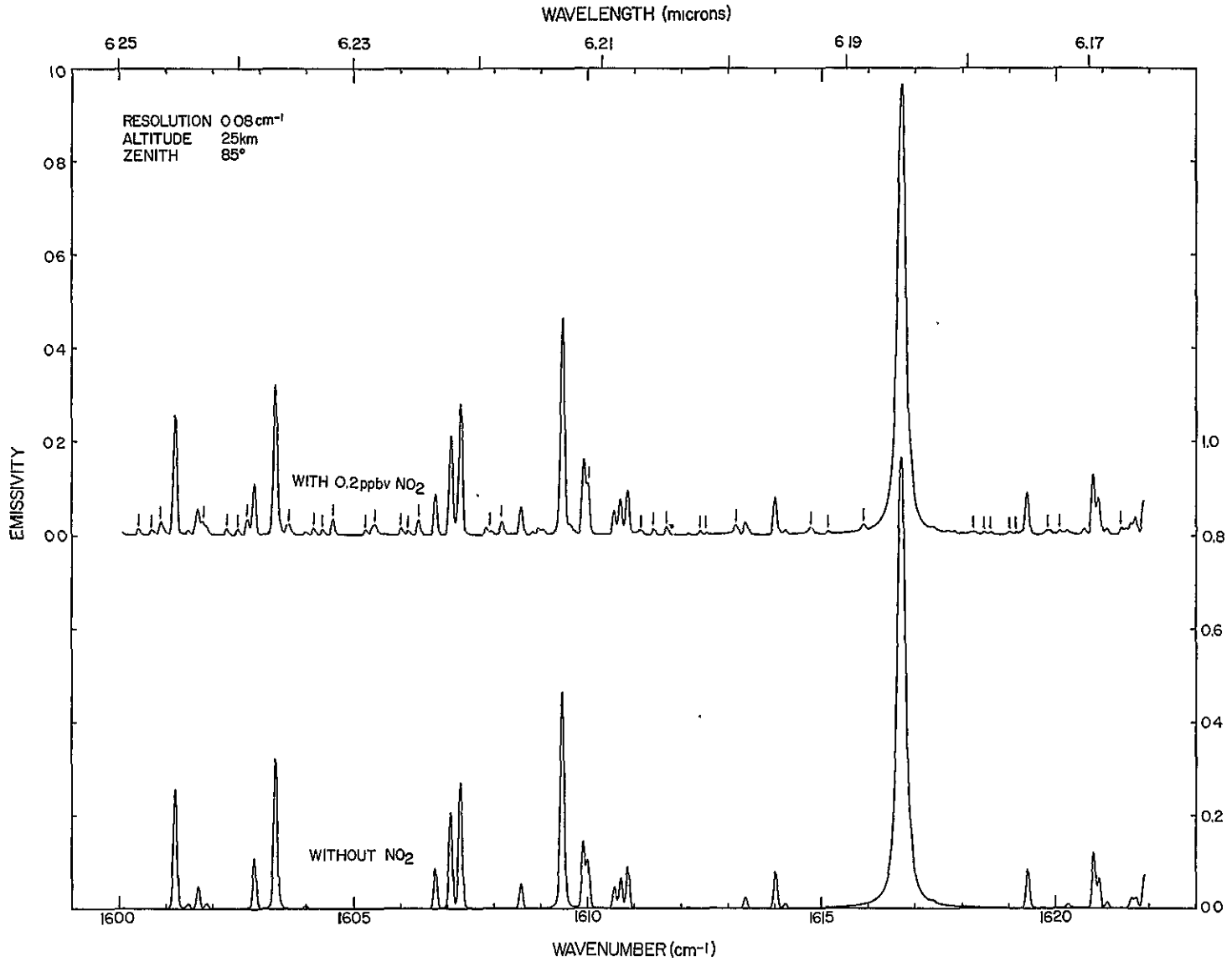
WAVELENGTH (microns)
6.25
6.23
6.21
6.19
6.17
RESOLUTION 0.08 cm⁻¹
ALTITUDE 25km
ZENITH 85°
WITH 0.2ppbv NO2
WITHOUT NO2
EMISSIVITY
1.0
0.8
0.6
0.4
0.2
0.0
1600
1605
1610
1615
1620
WAVENUMBER (cm⁻¹)

Figure 29.

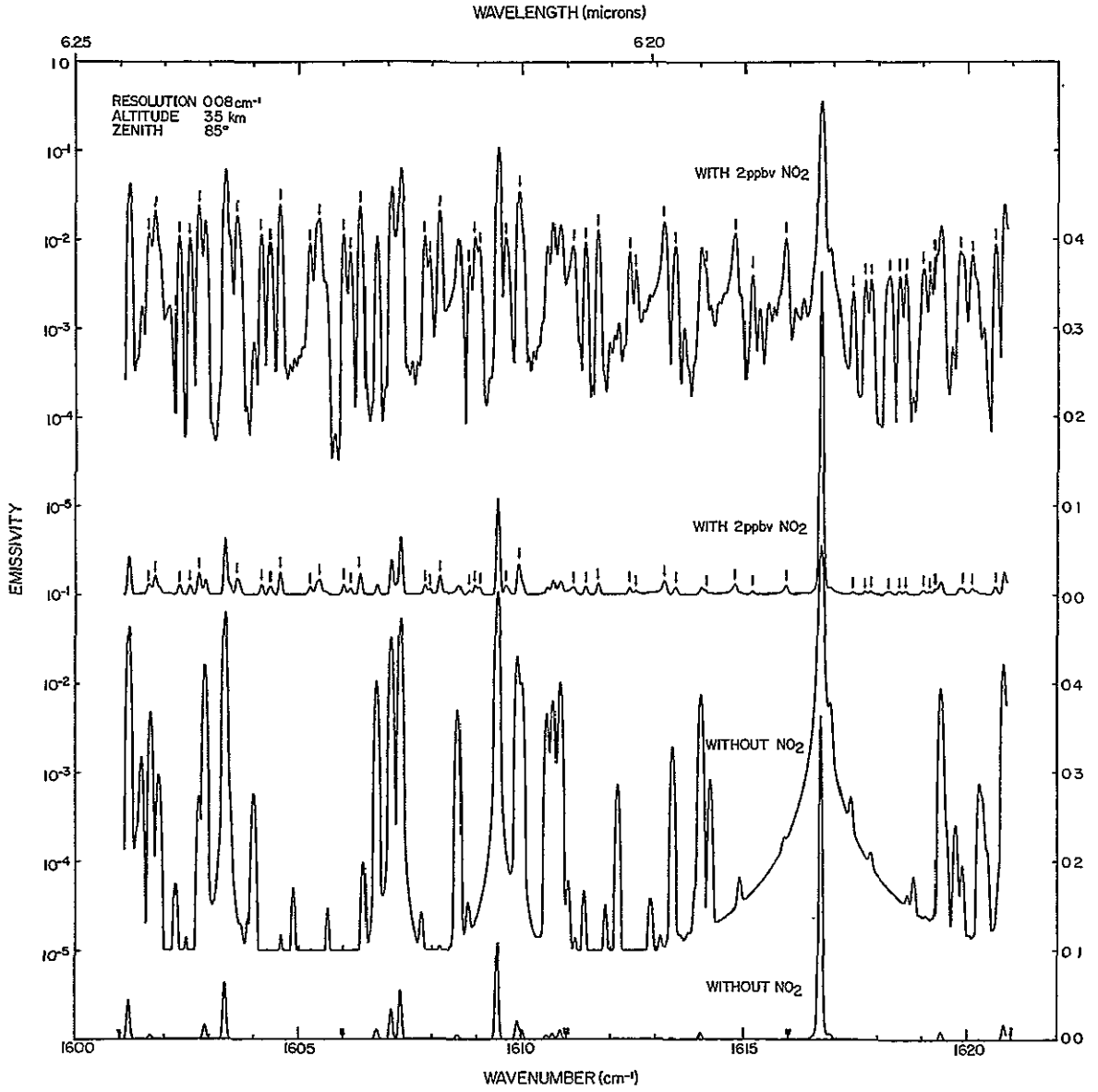
WAVELENGTH (microns)
6.25
6.20
RESOLUTION 0.08 cm⁻¹
ALTITUDE 35 km
ZENITH 85°
WITH 2ppbv NO2
WITH 2ppbv NO2
WITHOUT NO2
WITHOUT NO2
EMISSIVITY
1600
1605
1610
1615
1620
WAVENUMBER (cm⁻¹)

Figure 30.

III. H. SO_2

The ν_3 vibration-rotation fundamental band, with the strong Q-branch near 1360 cm^{-1}, is the strongest of the SO_2 bands.

The atmospheric spectral radiance calculated for a spectral radiometer at 5.5 km altitude, an 80° zenith angle and 1 cm^{-1} resolution (Figure 31) shows significant signal change with the addition of 10 ppbv SO_2. However, the spectrum is dominated by the background atmosphere and is also close to a blackbody spectrum. As a result no individual features of SO_2 can be isolated and the SO_2 contribution is manifested in small changes of the broad atmospheric peaks. Derivation of SO_2 amounts from atmospheric radiance measurements under such conditions is bound to have a very large uncertainty, despite the calculated large change in signal.

The situation is somewhat improved when similar calculations are made for 15 km altitude in Figure 32, however, most of the SO_2 features are still masked by the background atmospheric lines. The addition of 5 ppbv SO_2 to the atmosphere results in potentially measurable changes of the intensities of the atmospheric peaks.

In both of the above cases the atmospheric radiance levels are larger than 10^{-5} w $cm^{-2} sr^{-1} \mu m^{-1}$ and the absorptivities are between 10 and 50%. These are well within the capability of current instruments.

The atmospheric absorption spectra in a solar spectrum measurement from an altitude of 25 km , an 85° zenith angle and 0.08 cm^{-1} resolution show that the 1360 cm^{-1} region allows the measurement of ~0.5 ppbv SO_2 from ~1% absorptivity of isolated SO_2 peaks (Figures 33 and 34). These SO_2 peaks are a portion of the strong Q-branch of the ν_3 band. The SO_2 peaks near 1365 cm^{-1} also have potential for SO_2 measurements in the atmosphere.

The spectral region used here occurs at the wings of the 1326 cm^{-1} HNO_3 band (not included in the present calculations) and only a little interference is expected from this band. It should be noted, however, that the line parameters of the ν_3 SO_2 band have not been studied enough to guarantee the accuracy achieved for most of the other line parameters used in this study.

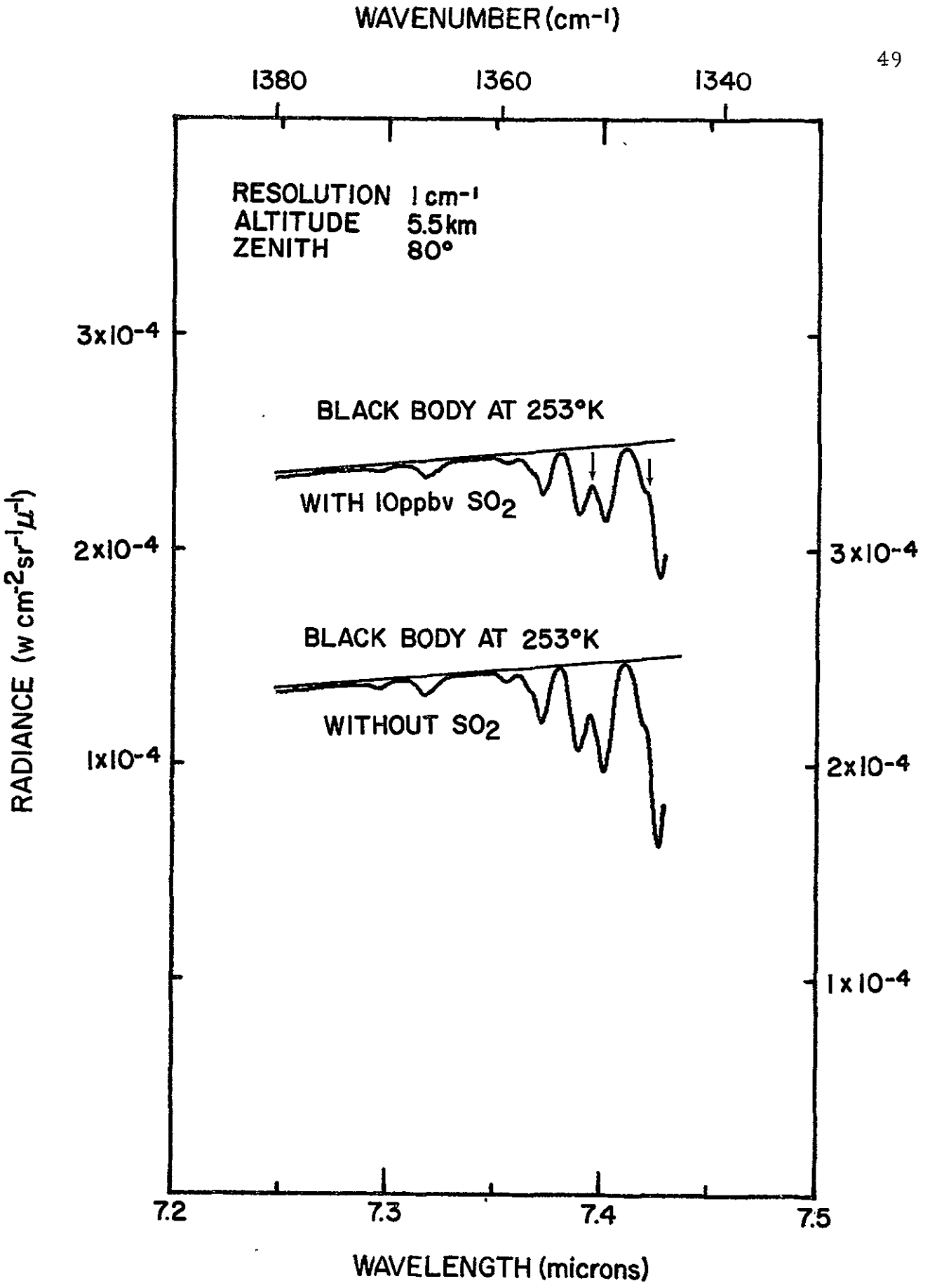
WAVENUMBER (cm-1)
1380
1360
1340
RESOLUTION 1 cm-1
ALTITUDE 5.5km
ZENITH 80°
BLACK BODY AT 253°K
WITH 10ppbv SO2
BLACK BODY AT 253°K
WITHOUT SO2
RADIANCE (w cm-2sr-1μ-1)
3x10-4
2x10-4
1x10-4
7.2
7.3
7.4
7.5
WAVELENGTH (microns)

Figure 31.

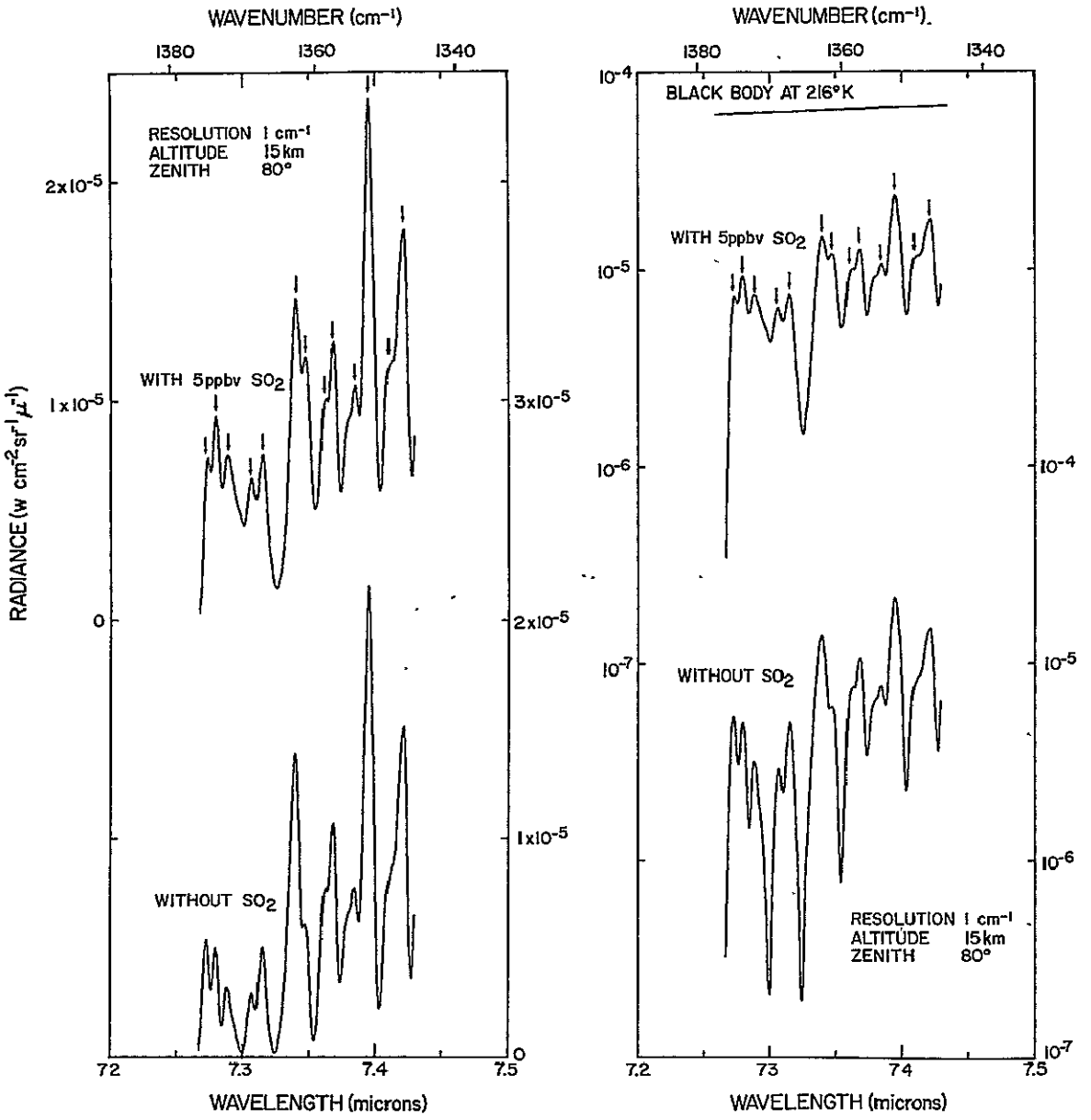
WAVENUMBER (cm⁻¹)
1380
1360
1340
RESOLUTION 1 cm⁻¹
ALTITUDE 15km
ZENITH 80°
WITH 5ppbv SO2
WITHOUT SO2
RADIANCE (w cm⁻² sr⁻¹ μ⁻¹)
2x10⁻⁵
1x10⁻⁵
0
3x10⁻⁵
2x10⁻⁵
1x10⁻⁵
0
7.2
7.3
7.4
7.5
WAVELENGTH (microns)
WAVENUMBER (cm⁻¹)
1380
1360
1340
BLACK BODY AT 216°K
WITH 5ppbv SO2
WITHOUT SO2
RESOLUTION 1 cm⁻¹
ALTITUDE 15km
ZENITH 80°
10⁻⁴
10⁻⁵
10⁻⁶
10⁻⁷
7.2
7.3
7.4
7.5
WAVELENGTH (microns)

Figure 32.

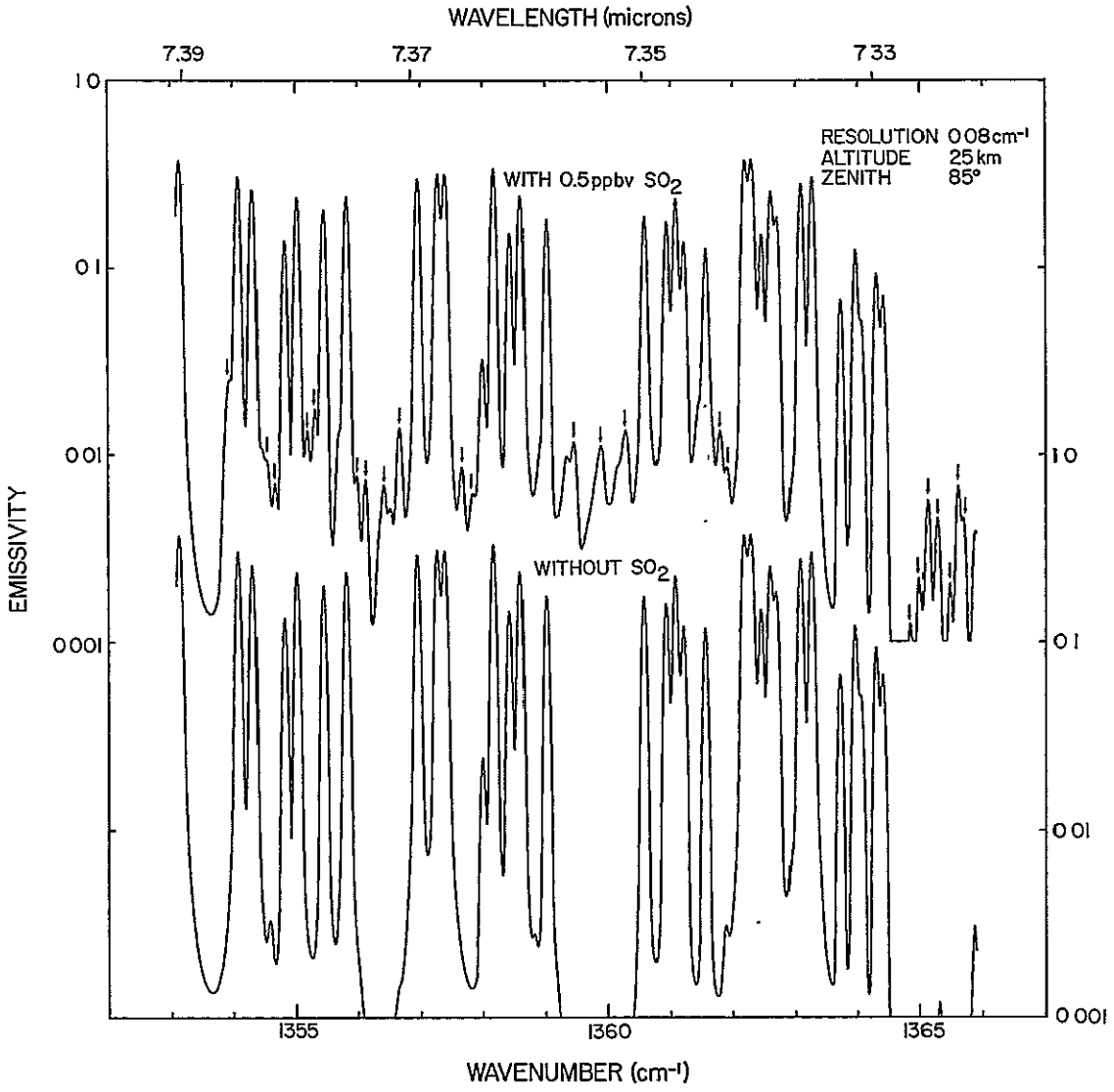
WAVELENGTH (microns)
7.39
7.37
7.35
7.33
1.0
0.1
0.01
0.001
EMISSIVITY
RESOLUTION 0.08cm⁻¹
ALTITUDE 25km
ZENITH 85°
WITH 0.5ppbv SO_2
WITHOUT SO_2
1355
1360
1365
WAVENUMBER (cm⁻¹)

Figure 33.

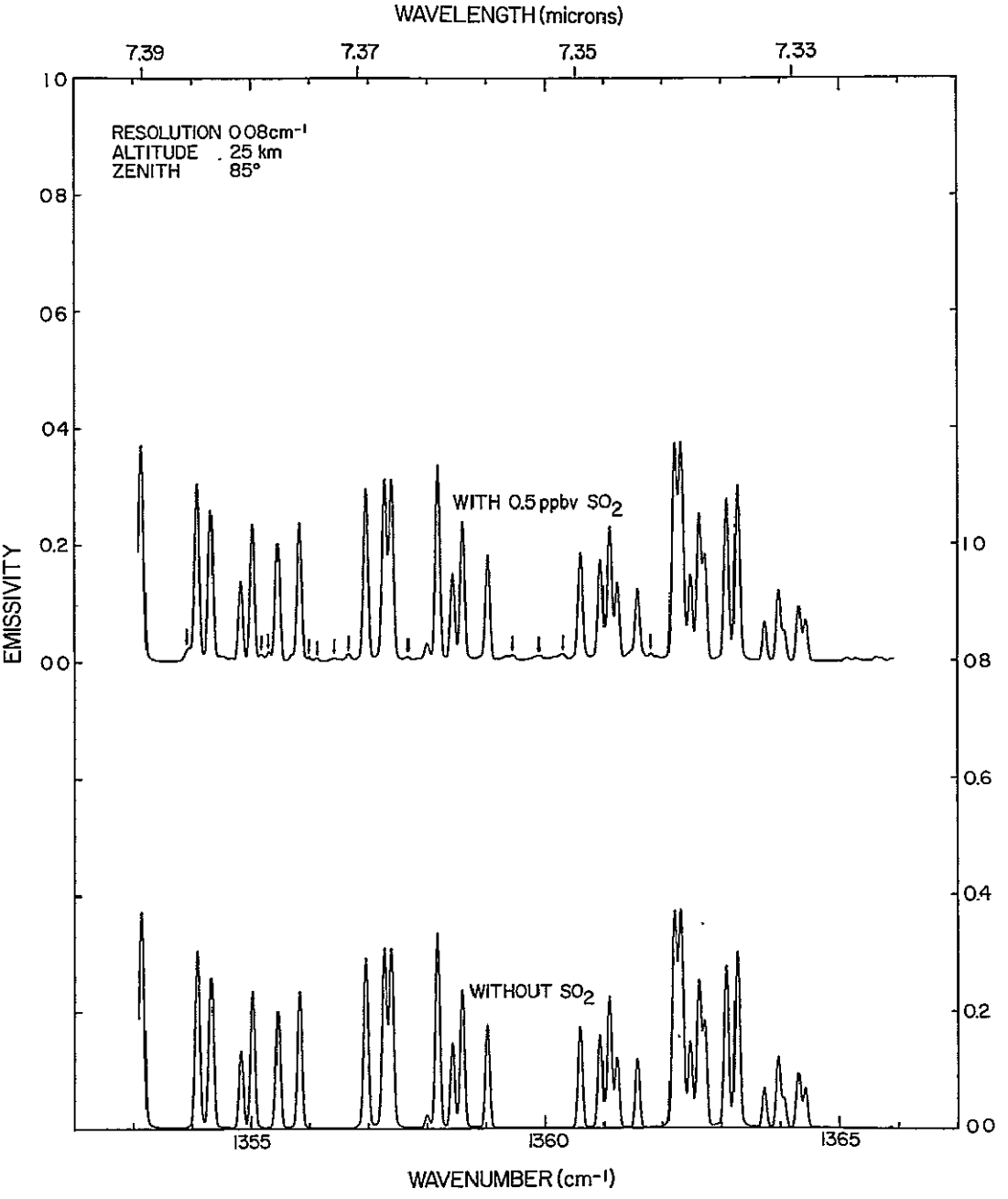
WAVELENGTH (microns)
7.39
7.37
7.35
7.33
RESOLUTION 0.08cm⁻¹
ALTITUDE 25 km
ZENITH 85°
WITH 0.5 ppbv SO2
WITHOUT SO2
EMISSIVITY
1.0
0.8
0.6
0.4
0.2
0.0
1355
1360
1365
WAVENUMBER (cm⁻¹)

Figure 34.

IV. Discussion

The limits of detectability of the particular constituents discussed above are somewhat arbitrary and are based on the authors' extensive experience with infrared transmittance and radiance measurements and, to a lesser extent, their familiarity with other measurements. It is felt that the detection limits quoted are realistic estimates of what can be done with current instrumentation. The use of a detection limit of 1% absorption in the case of atmospheric absorption using the sun as a source is based on the fact that it is close to the limit achieved in the data published to date.

Examination of the calculated spectra indicate that the combination of resolution and long optical path that can be achieved using the sun as a source during sunset (or sunrise) is a particularly sensitive technique for detection of small amounts of a trace constituent. This technique is particularly useful above the tropopause where interference effects are significantly reduced. As the sensitivity of spectral radiometer systems increases, the advantage of atmospheric absorption (solar spectra) technique, over the atmospheric emission technique, diminishes. When other considerations are taken into account (cost, time of day measurements are needed, data reduction, etc.) quite often the emission technique is better suited for the desired measurement. At the lower altitudes where atmospheric background absorptions start to significantly mask the absorptions due to the desired constituent, the long path absorption cell technique often will be suitable for obtaining data when the other techniques are not. Thus, it is not possible to say that one of the three techniques is the best technique for measuring minor constituents.

Several remarks should be made regarding the spectra presented above. The spectral regions which were selected for use in this study were chosen from the strongest vibration-rotation bands for the molecule having the minimum interference in the region from the "background" constituents. These choices were based on the extensive balloon observations of the variation of atmospheric infrared emission and absorption spectra altitude made by our group along with those of other groups.

No claim is made of completeness in examining any of the parameters of the eight constituents discussed here. Each has many spectral regions which might be useful, while only the stronger spectral transitions were considered here. Most are presumed to have variable mixing ratios with altitude and in the event they are strongly layered, there is undoubtedly a more unique experiment and calculations which could be performed. No consideration of aerosols has been made here, which undoubtedly effects low level emissivity measurements.

It must be emphasized that the concept of detectable limits is not uniquely defined. The calculated spectra demonstrate that the detectable limit depends on the physical parameters of the experimental environment as well as the specific experimental technique. The gas amount denoted in each figure was chosen because it exhibits weak but observable spectral features, allowing an estimate of the minimum detectable amount under the specified experimental conditions. The detectable gas amount depends strongly on the interference with other spectral lines and on the uncertainties in the spectral line parameters of both the background atmosphere and the constituent. These can vary significantly from one case to another, according to path, altitude, spectral region and resolution, from completely isolated

spectral lines of a constituent to lines that are completely masked by the background atmosphere.

In several cases shown here the presence of a constituent on the atmospheric spectrum is manifested not by a unique fine structure, but rather in a change of the intensity of patterns that already exist in the background atmospheric spectrum. Meaningful measurements of trace constituents under such conditions require significantly larger minimum detectable amounts to overcome the uncertainty involved in the measurements and in the theoretical interpretations of the atmospheric spectral patterns.

Finally, the spectral plots given here can be used to estimate the possibility of detection of a different amount of the trace constituents under different experimental conditions by interpolation between the various figures. Such interpolation must be done with care since simple linear interpolation is accurate only if the constituent absorption lines show a few percent absorptivity ($\lesssim 10\%$) at "infinite" resolution. A similar remark applies to changes in the interfering background lines.

Acknowledgments

Acknowledgment is made to the National Center for Atmospheric Research which is sponsored by the National Science Foundation, for computer time used in this research. The NO_2 and SO_2 line parameters were kindly prepared by D. E. Snider. The NH_3 line parameters were kindly made available by F. W. Taylor. Many helpful contributions were made by D. B. Barker, J. N. Brooks, J. J. Kosters, F. H. Murcray and J. Van Allen. The figures were carefully prepared by Carolyn Bauer.

References

1. C. B. Ludwig, R. Bartle and M. Griggs, "Study of Air Pollutant Detection by Remote Sensors," NASA CR-1380, July 1969.

2. "Monitoring of Air Pollution by Satellites (MAPS)," (Phase I) Final Report NASA CR-112137, April 1972, Convair Aerospace Division, General Dynamics Corporation, San Diego, California.

3. C. B. Ludwig, M. Griggs, W. Malkmus and E. R. Bartle, "Air Pollution Measurements from Satellites," NASA CR-2324, Nov. 1973, Convair Aerospace Division, General Dynamics Corporation, San Diego, California.

4. C. B. Ludwig, M. Griggs, W. Malkmus and E. R. Bartle, "Measurement of Air Pollutants from Satellites. 1: Feasibility Considerations," Appl. Opt. 13, 1494 (1974).

5. S. R. Drayson, F. L. Bartman, W. R. Kuhn and R. Tallamraju, "Satellite Measurement of Stratospheric Pollutants and Minor Constituents by Solar Occulatation: A Preliminary Report," Final Report 011023-1-T, Nov. 1972, National Oceanic and Atmospheric Administration Grant NG-10-72, High Altitude Engineering Laboratory, Departments of Aerospace Engineering, Atmospheric and Oceanic Science, University of Michigan, Ann Arbor, Michigan.

6. C. B. Farmer, R. A. Toth, R. A. Schindler and O. F. Raper, "Near-Infrared Interferometric Measurements of Stratospheric Composition to be Made from the Concorde," p. 65, Proceedings of the Second Conference on the Climatic Impact Assessment Program, Nov. 14-17, 1972, A. J. Broderick, Editor.

7. L. D. Kaplan, "Background Concentrations of Photochemically Active Trace Constituents in the Stratosphere and Upper Troposphere," Pure and Appl. Geophys. 106-108, 1341 (1973).

8. C. B. Farmer, "Infrared Measurements of Stratospheric Composition," Canad. J. Chem. 52, 1544 (1974).

9. P. L. Hanst, "Infrared Spectroscopy and Infrared Lasers in Air Pollution Research and Monitoring," Appl. Spectrosc. 24, 161 (1970).

10. P. L. Hanst, A. F. Lefohn and B. W. Gay, Jr., "Detection of Atmospheric Pollutants at Parts-per-Billion Levels by Infrared Spectroscopy" Appl. Spectrosc. 27, 188 (1973).

11. R. T. Menzies, "Use of CO and CO_2 Lasers to Detect Pollutants in the Atmosphere," Appl. Opt. 7, 1532 (1971).

12. R. T. Menzies and M. S. Shumate, "Air Pollution: Remote Detection of Several Pollutant Gases with a Laser Heterodyne Radiometer," Science 184, 570 (1974).

13. L. B. Kreuzer, N. D. Kenyon and C. K. N. Patel, "Air Pollution: Sensitive Detection of Ten Pollutant Gases by Carbon Monoxide and Carbon Dioxide Lasers," Science 177, 347 (1972).

14. C. Chackerian, Jr. and M. F. Weisbach, "Amplified Laser Absorption: Detection of Nitric Oxide," J. Opt. Soc. Am. 63, 342 (1972).

15. E. D. Hinkley, "Bistatic Monitoring of Gaseous Pollutants with Tunable Semiconductor Lasers," Symposium on Remote Sensing of Environmental Air Pollutants at the 1974 Pittsburgh Conference on Analytical Chemistry and Applied Spectroscopy, Cleveland, Ohio, 7 March 1974.

16. K. G. P. Sulzmann, J. E. L. Lowder and S. S. Penner, "Estimates of Possible Detection Limits for Combustion Intermediates and Products with Line-Center Absorption and Derivative Spectroscopy using Tunable Lasers," Combustion and Flame 20, 177 (1973).

17. H. W. Goldstein, M. H. Bortner, R. N. Grenda, A. M. Karger and P. J. LeBel, "Correlation Interferometric Measurement of Trace Species in the Atmosphere," AIAA Paper No. 73-515 (1973).

18. C. R. McCreight and C. L. Tien, "Low-Resolution Infrared Derivative Spectrometry for Source Concentration Monitoring, J. Quant. Spectrosc. Radiat. Transfer 13, 1143 (1973).

19. D. G. Murcray, A. Goldman, W. J. Williams, F. H. Murcray, J. Van Allen and S. C. Schmidt, "Observations of the Solar Spectrum in the 1800-2100 cm^{-1} Region and the Search for NO Lines," p. 246, Proceedings of the Third Conference on the Climatic Impact Assessment Program, Feb. 26-March 1, 1974, A. J. Broderick and T. M. Hard, Editors.

20. R. A. McClatchey, R. W. Fenn, J. E. A. Selby, F. E. Volz and J. S. Garing, "Optical Properties of the Atmosphere," Third Ed. AFCRL-72-0497, 24 Aug. 1972, Environmental Research Papers No. 411, Air Force Cambridge Research Laboratories, L. G. Hanscom Field, Bedford, Massachusetts 01730.

21. R. A. McClatchey, W. S. Benedict, S. A. Clough, D. E. Burch, R. F. Calfee, K. Fox, L. S. Rothman and J. S. Garing, "AFCRL Atmospheric Absorption Line Parameters Compilation," AFCRL-TR-73-0096, 26 Jan. 1973, Environmental Research Papers, No. 434, Air Force Cambridge Research Laboratories, L. G. Hanscom Field, Bedford, Massachusetts 01730.

22. A. Goldman, R. M. Blunt and J. R. Riter, "IR Spectrum Simulating Pyrotechnics," Report 4958-7405-2Q, Contract N00019-74-C-00051, Naval Air Systems Command, by Denver Research Institute, University of Denver, Denver, Colorado 80210.

23. A. Goldman, S. C. Schmidt, J. R. Riter and R. M. Blunt, "Infrared Spectral Radiance of Hot HF and DF in the $\Delta v = 1$ Region as Seen Through an Atmospheric Path," J. Quant. Spectrosc. Radiat. Transfer 14, 299 (1974).

24. F. W. Taylor, "Spectral Data for the ν_2 Bands of Ammonia with Applications to Radiative Transfer in the Atmosphere of Jupiter," J. Quant. Spectrosc. Radiat. Transfer 13, 1181 (1973).

25. A. Goldman and S. C. Schmidt, "Infrared Spectral Line Parameters and Absorptance Calculations of NO at Atmospheric and Elevated Temperatures for the $\Delta v = 1$ Bands Region," J. Quant. Spectrosc. Radiat. Transfer, 15, 127 (1975).

26. A. Goldman, F. S. Bonomo, W. J. Williams, D. G. Murcray and D. E. Snider, "Absolute Integrated Intensity and Individual Line Parameters for the 6.2μ Band of NO_2," J. Quant. Spectrosc. Radiat. Transfer, 15, 107 (1975).

27. K. Fox, G. D. T. Tejwani and R. J. Corice, Jr., "Fundamental Bands of $^{32}S\,^{16}O_2$, "Research Report No. UTPA-ERAL-01, Sept. 1972, Earth Resources and Astrophysics Laboratory, Department of Physics and Astronomy, The University of Tennessee, Knoxville, Tennessee 37916.

28. R. J. Corice, Jr., K. Fox and G. D. T. Tejwani, "Experimental and Theoretical Studies of the Fundamental Bands of Sulfur Dioxide," J. Chem. Phys. 58, 265 (1973).

29. D. G. Murcray, F. H. Murcray and W. J. Williams, "High Altitude Atmospheric Transmittance as Observed over Northern California," AFCRL-66-410, Scientific Report No. 3, May 1966, Dept. of Physics, University of Denver, Denver, Colorado 80210.

30. D. G. Murcray, F. H. Murcray and W. J. Williams, "Atmospheric Absorptions Over Long Slant Paths in the Stratosphere," AFCRL-66-812, Scientific Report No. 4, October 1966, Dept. of Physics, University of Denver, Denver, Colorado 80210.

31. D. G. Murcray, T. G. Kyle, F. H. Murcray and W. J. Williams, "Nitric Acid and Nitric Oxide in the Lower Stratosphere," Nature, 218, 78 (1968).

32. D. G. Murcray, F. H. Murcray, W. J. Williams, T. G. Kyle and A. Goldman, "Variation of the Infrared Solar Spectrum Between 700 cm^{-1} and 2240 cm^{-1} with Altitude," Appl. Opt. 8, 2519 (1969).

33. W. J. Williams, F. H. Murcray, D. G. Murcray and T. G. Kyle, "Flow of Radiation in the Earth's Atmosphere," AFCRL-70-0415 Final Report, Jan. 1970, Dept. of Physics, University of Denver, Denver, Colorado 80210.

34. A. Goldman, D. G. Murcray, F. H. Murcray, W. J. Williams and F. S. Bonomo, "Identification of the ν_3 NO_2 Band in the Solar Spectrum Observed from a Balloon-Borne Spectrometer," Nature 225, 443 (1970).

35. D. G. Murcray, D. B. Barker, J. N. Brooks, J. J. Kosters, F. H. Murcray and W. J. Williams, "Atmospheric Emission at High Altitudes," AFCRL-72-0353, Final Report, June 1972, Dept. of Physics, University of Denver, Denver, Colorado 80210.

36. J. N. Brooks, A. Goldman. J. J. Kosters, D. G. Murcray, F. H. Murcray and W. J. Williams, "Balloon-Borne Infrared Measurements," in Physics and Chemistry of Upper Atmospheres, B. M. McCormac (Ed.), p. 278, (1973).

37. D. G. Murcray, A. Goldman, F. H. Murcray, W. J. Williams, J. N. Brooks and D. B. Barker, "Vertical Distribution of Minor Atmospheric Constituents as Derived from Air-Borne Measurements of Atmospheric Emission and Absorption Infrared Spectra," AIAA paper No. 73-103, 1973.

38. D.G. Murcray, A. Goldman, W.J. Williams, F.H. Murcray, J.N. Brooks, J. Van Allen, R.N. Stocker, J.J. Kosters, D.B. Barker and D.E. Snider, "Recent Results of Stratospheric Trace Gas Measurements from Balloon-Borne Spectrometers" p. 184, Proceedings of the Third Conference on the Climatic Impact Assessment Program, Feb. 26-March 1, 1974, A.J. Broderick and T.M. Hard, Editors.

39. M. Migeotte, L. Neven and J. Swensson, "The Solar Spectrum from 2.8 to 23.7 Microns' Part I. Photometric Atlas, Mém. Soc. Roy. Sci. Liège, Spec. Vol. 1 (1956); Part II. Measures and Identifications, Mém. Soc. Roy. Sci. Liège, Vol. 2 (1957).

40. A. Goldman, F.S. Bonomo, W.J. Williams and D.G. Murcray, "Statistical-Band-Model Analysis and Integrated Intensity for the 21.8μm Bands of HNO_3 Vapor" J. Opt. Soc. Am. 65, 10 (1975)..

41. J.C. Fontanella, A. Girard. L. Gramont and N. Louisnard, "Vertical Distribution of NO, NO_2 and HNO_3 as Derived from Stratospheric Absorption Infrared Spectra" p. 217, Proceedings of the Third Conference on the Climatic Impact Assessment Program, Feb. 26-March 1, 1974, A.J. Broderick and T.M. Hard, Editors.

42. D.G. Murcray, A. Goldman, A. Csoeke-Poeckh, F.H. Murcray, W.J. Williams and R.N. Stocker, "Nitric Acid Distribution in the Stratosphere" J. Geophys. Res. 78, 7033 (1973).